HAL open science

Sea Ice CO2 Dynamics Across Seasons: Impact of Processes at the Interfaces

F. van Der Linden, Jean-Louis Tison, W. Champenois, S. Moreau, Gautiher Carnat, M. Kotovitch, François Fripiat, F. Deman, A. Roukaerts, Frank Dehairs, et al.

To cite this version:

F. van Der Linden, Jean-Louis Tison, W. Champenois, S. Moreau, Gautiher Carnat, et al.. Sea Ice CO2 Dynamics Across Seasons: Impact of Processes at the Interfaces. Journal of Geophysical Research. Oceans, 2020, 125 (6), 10.1029/2019jc015807 . hal-03035303

HAL Id: hal-03035303

https://hal.science/hal-03035303

Submitted on 22 Jun 2022

HAL is a multi-disciplinary open access archive for the deposit and dissemination of scientific research documents, whether they are published or not. The documents may come from teaching and research institutions in France or abroad, or from public or private research centers.

L'archive ouverte pluridisciplinaire **HAL**, est destinée au dépôt et à la diffusion de documents scientifiques de niveau recherche, publiés ou non, émanant des établissements d'enseignement et de recherche français ou étrangers, des laboratoires publics ou privés.

Copyright

Check for updates

ADVANCING EARTH AND SPACE SCIENCE

JGR Oceans

RESEARCH ARTICLE
10.1029/2019JC015807

Key Points:
- First long-term monitoring of both pCO_2 and CO_2 fluxes at sea ice interfaces in McMurdo Sound (Antarctica) from late winter to summer
- Large biomass build-up is strikingly associated with transient heterotrophy and nitrate plus nitrite accumulation
- New conceptual approach involving biofilm formation can explain observed inconsistencies: accumulation of nitrate plus nitrite and $CaCO_3$

Supporting Information:
- Supporting Information S1

Correspondence to:
F. C. Van der Linden,
fvanderlinden@uliege.be

Citation:
Van der Linden, F. C., Tison, J.-L., Champenois, W., Moreau, S., Carnat, G., Kotovitch, M., et al. (2020). Sea Ice CO_2 Dynamics Across Seasons: Impact of Processes at the Interfaces. *Journal of Geophysical Research: Oceans*, *125*, e2019JC015807. https://doi.org/10.1029/2019JC015807

Received 23 OCT 2019
Accepted 5 MAY 2020
Accepted article online 13 MAY 2020

©2020. American Geophysical Union. All Rights Reserved.

Sea Ice CO_2 Dynamics Across Seasons: Impact of Processes at the Interfaces

F. C. Van der Linden[1,2], J.-L. Tison[2], W. Champenois[1], S. Moreau[3], G. Carnat[2], M. Kotovitch[1,2], F. Fripiat[2], F. Deman[1,4], A. Roukaerts[4], F. Dehairs[4], S. Wauthy[2], A. Lourenço[5], F. Vivier[5], T. Haskell[6], and B. Delille[1]

[1]Unité d'océanographie chimique, MARE, Université de Liège, Liège, Belgium, [2]Laboratoire de Glaciologie, DGES, Université Libre de Bruxelles, Brussels, Belgium, [3]Norwegian Polar Institute, Tromsø, Norway, [4]Analytical, Environmental, and Geochemistry, Earth Sciences Research Group, Vrije Universiteit Brussel, Brussels, Belgium, [5]LOCEAN-IPSL, Sorbonne Universités (UPMC Paris 6), CNRS, Paris, France, [6]Callaghan Innovation, Wellington, New Zealand

Abstract Winter to summer CO_2 dynamics within landfast sea ice in McMurdo Sound (Antarctica) were investigated using bulk ice pCO_2 measurements, air-snow-ice CO_2 fluxes, dissolved inorganic carbon (DIC), total alkalinity (TA), and ikaite saturation state. Our results suggest depth-dependent biotic and abiotic controls that led us to discriminate the ice column in three layers. At the surface, winter pCO_2 supersaturation drove CO_2 release to the atmosphere while spring-summer pCO_2 undersaturation led to CO_2 uptake most of the time. CO_2 fluxes showed a diel pattern superimposed upon this seasonal pattern which was potentially assigned to either ice skin freeze-thaw cycles or diel changes in net community production. In the ice interior, the pCO_2 decrease across the season was driven by physical processes, mainly independent of the autotrophic and heterotrophic phases. Bottom sea ice was characterized by a massive biomass build-up counterintuitively associated with transient heterotrophic activity and nitrate plus nitrite accumulation. This inconsistency is likely related to the formation of a biofilm. This biofilm hosts both autotrophic and heterotrophic activities at the bottom of the ice during spring and may promote calcium carbonate precipitation.

Plain Language Summary Sea ice participates actively in the regional cycling of CO_2 both as a source and a sink at different times of the year depending on ice physics, ice chemistry, and ice trophic status (autotrophic vs. heterotrophic). We identified the key processes driving the CO_2 dynamics in each sea ice layer (surface, interior, and bottom) from McMurdo Sound (Antarctica) from late winter to summer. At the surface, CO_2 release from the ice to the atmosphere occurred in late winter while CO_2 uptake occurred in summer. Superimposed upon this seasonal pattern, we observed a diurnal pattern with both release and uptake occurring over 24 hr period. This diurnal pattern can be related to physical processes (nocturnal freeze-up and diurnal melting) or biotic processes (autotrophy or heterotrophy). In the ice interior, a succession of autotrophic and heterotrophic phases took place. At the sea ice bottom, a particular assemblage of microbial cells and organic matter, called biofilm, enabled the accumulation of biomass and nitrate plus nitrite simultaneously leading to both autotrophic and heterotrophic activities. In addition, this biofilm is suggested to promote calcium carbonate precipitation.

1. Introduction

Over the global oceans, polar oceans act as a major sink for atmospheric CO_2 (Gruber et al., 2019; Takahashi et al., 2002), with air-sea fluxes estimated at −199 Tg C year^{-1} (Rysgaard et al., 2011). At high latitudes, the CO_2 cycle is strongly affected by the presence of sea ice. More than just an interface affecting gas transfers, sea ice is also one of the most extensive and dynamic ecosystems that consumes and produces CO_2. Over the last decade, studies highlighted the complex role of sea ice in CO_2 exchanges and reported CO_2 fluxes over sea ice ranging from −5.4 to +9.9 μmol m^{-2} day^{-1}, with a negative value indicating CO_2 uptake and a positive value indicating CO_2 release from the ice to the atmosphere (supporting information Table S1). Fluxes have been documented mainly in spring and summer (Brown et al., 2015; Delille et al., 2014; Geilfus et al., 2012, 2013, 2014, 2015; Nomura et al., 2010, 2013). No studies have examined the winter CO_2 exchanges above sea ice in Antarctica-a prerequisite to budget air-ice CO_2 fluxes over the whole year.

The partial pressure of CO_2 (pCO_2) within sea ice is a highly relevant parameter to understand the carbonate system. Factors affecting the sea ice pCO_2 include biotic (e.g., primary production and respiration; Delille et al., 2007) and abiotic (e.g., CO_2 transport and exchanges, freezing, melting, calcium carbonate precipitation and dissolution; Rysgaard et al., 2007) processes. The strong seasonality of these biotic and abiotic processes in brine inclusions, coupled with the thermodynamically driven evolution of brine inclusions volume, salinity, and connectivity, lead to strong temporal variability in the sea ice CO_2 dynamics (Geilfus, Delille, et al., 2012; Papadimitriou et al., 2012).

The gradient of pCO_2 between the ice and the atmosphere is driving CO_2 exchanges, controlling both the fluxes direction and magnitude. Ice-atmosphere CO_2 exchanges are moreover strongly affected by the conditions at the interface, including ice type (superimposed ice, snow ice, and granular ice), presence or absence of snow cover, and the ice and snow chemical and physical properties. Snow salinity, wetness, density, and grain sizes among others are likely to affect the magnitude and direction of CO_2 fluxes (Delille et al., 2014; Nomura et al., 2018; Nomura, Yoshikawa-Inoue, et al., 2010). The presence of brine within the snowpack is induced by four processes: flooding, brine wicking, frost flowers formation, and aerosols deposition (Domine et al., 2004; Massom et al., 2001). Brine-wetted snow is a multiphase reactor hosting specific physical and chemical processes that may influence CO_2 fluxes: uptake and migration of trace gas, diffusion, and sources and sinks processes (Bartels-Rausch et al., 2014). While the impact of fresh snow cover on gas fluxes has been documented for terrestrial environments (Brooks et al., 2005; Takagi et al., 2005), the role of the snow on sea ice is still overlooked.

As a biome, sea ice provides a dynamic habitat for diverse communities of microorganisms including algae, bacteria, heterotrophic protists, fungi, and viruses (Deming, 2010; Horner et al., 1992; Luhtanen et al., 2018; Poulin et al., 2011; Thomas & Dieckmann, 2010). In landfast sea ice, that is, immobile sea ice anchored either to coasts or continental ice formations or grounded over shoals (Meiners et al., 2018), communities are mainly concentrated either at the bottom of the ice or within a loose and unconsolidated layer of ice crystals, known as platelet underneath the columnar ice (Arrigo et al., 1995). Platelet ice is formed in supercooled waters observed around Antarctic ice shelves (Jeffries et al., 1993; Leonard et al., 2006). Bacterial and algal production affect the CO_2 dynamics by releasing or consuming CO_2, impacting concentrations of dissolved inorganic carbon (DIC) and total alkalinity (TA)-key parameters that drive the ocean-sea ice-atmosphere CO_2 fluxes. In oxic conditions, apart from the calcification, the contribution of microbial processes to DIC changes is best described by the net community production (NCP). NCP corresponds to the balance between photosynthesis and respiration of all organisms and determines the net trophic status of the ice (autotrophic vs. heterotrophic). Positive NCP (autotrophy) leads to a consumption of DIC and a production of O_2, whose stoichiometry is tightened to photosynthetic and respiratory reactions (i.e., photosynthetic quotient) (Anderson, 1995; Glud et al., 2002). Some studies documented the net community production across the Arctic using standard measurement methods such as incubation of melted ice cores (Campbell et al., 2017; Søgaard et al., 2010) and highlighted succession of distinct heterotrophic and autotrophic phases. However, the processes and conditions in which heterotrophy or autotrophy dominates remain unclear.

Considering the lack of long-term and diurnal surveys of sea ice CO_2 dynamics and the need to integrate the full development of a microalgae bloom, we present results from a year-round survey of landfast sea ice carbon dynamics in Cape Evans, McMurdo Sound (Antarctica). We report O_2 and pCO_2 profiles within bulk sea ice as well as seasonal and diel patterns of CO_2 fluxes at the air-snow-ice interface. The potential for calcium carbonate precipitation is also investigated. We further examine chlorophyll a (chl-*a*) abundance, particulate organic carbon (POC), nitrate plus nitrite concentrations, and DIC changes over the bloom. We also compare these parameters with estimates of NCP and related ice trophic status.

2. Materials and Methods

2.1. Study Site and Sampling Scheme

Year-round survey of Ocean-Sea Ice-Atmosphere Exchanges (YROSIAE) was a temporal survey at one single ice location at Cape Evans (77°38′S, 166°23′E), on the eastern side of McMurdo Sound, Antarctica (Figure 1). Sampling was supported by Scott Base facilities and carried out in two phases, from November to December 2011 and from September to December 2012. The sampling area is characterized by the annual occurrence of

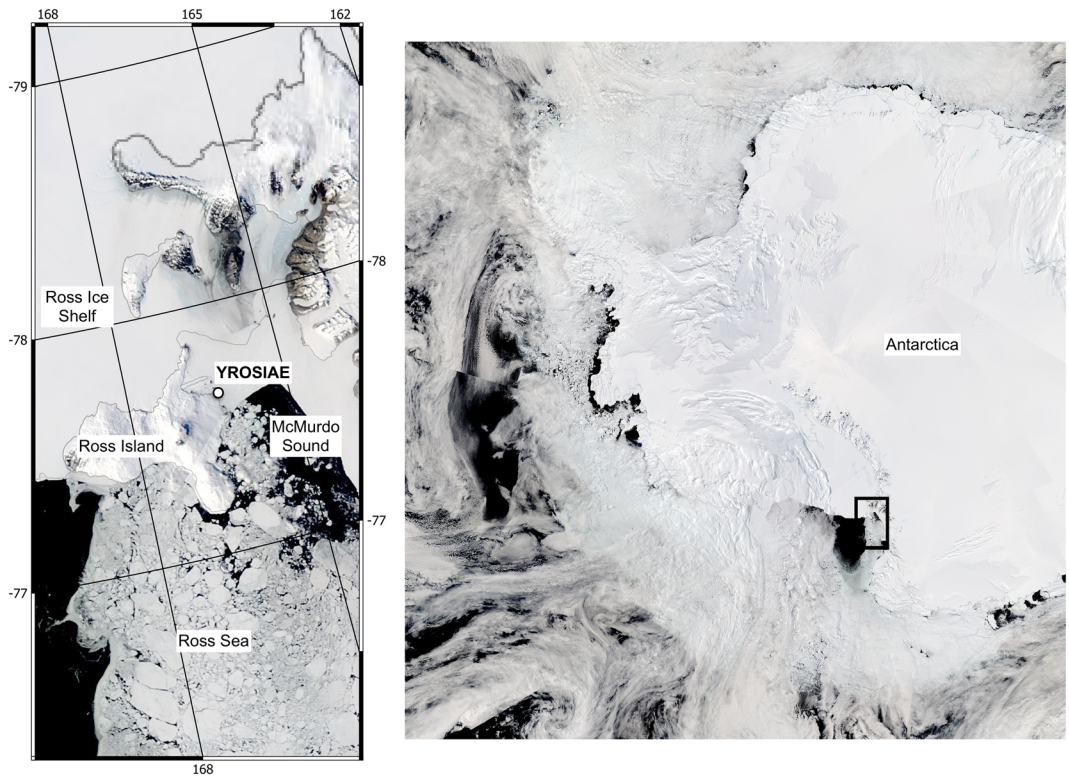

Figure 1. Location of the YROSIAE year-round sea ice biogeochemistry station, along Ross Island, Ross Sea, Antarctica. The satellite picture is a visible image from NASA's moderate resolution imaging Spectroradiometer (MODIS) Terra on 29 November 2012.

smooth, thick first-year landfast ice. Ice retreat began in early February 2012 in Cape Evans, and the area remained ice-free until the beginning of April 2012, approximatively 5 months before the second sampling phase (19 September 2012). Ice cores, snow, and seawater samples were collected during 12 ice stations. For the sake of consistency with other reports of YROSIAE results (Carnat et al., 2014, 2018), each station number, referenced hereafter as YRS#, corresponds to a dedicated sampling date as indicated in Figure 2 and in Table 1. Each time the site was visited, a new sampling square area of 10 m^2 was delimitated next to the sampling site of the previous station in order to minimize the bias from spatial heterogeneity. The snow cover was first sampled using plastic scoops and LDPE bottles, and then the ice coring started. Ice cores were collected using an electropolished stainless steel ice corer (14 cm ID). Immediately after drilling, cores were sealed in polyethylene bags and stored in a box containing −30°C frozen bags. Attention was paid to prevent brine drainage by keeping ice cores horizontally. Seawater sampling through core holes was performed at three different depths (0, 1, and 30 m) using a peristaltic pump (Cole Palmer, MasterflexVR- Environmental sampler) with Tygon® tubing.

Outside the sampling site, one soil CO_2 flux system was deployed with two long-term deployment automatic chambers. Chambers for CO_2 fluxes measurements were deployed over the snow and ice surfaces and were continuously running until they were blocked by the snowdrift. Every 4 to 7 days, maintenance and repositioning of the chambers on an unaltered surface were performed. From September to December 2012, an ice-T ice mass balance buoy developed at LOCEAN (UPMC, Paris) provided continuous measurements of air temperature and ice temperature at different depths. The experimental setting and sampling scheme are also detailed in Carnat et al. (2014).

2.2. Measured Parameters

2.2.1. Physical Parameters

In situ ice temperature was measured on ice cores immediately after sampling with a vertical resolution of 5 cm using a calibrated probe TESTO® 720 (precision ±0.1°C, accuracy ±0.2°C). Bulk ice salinity

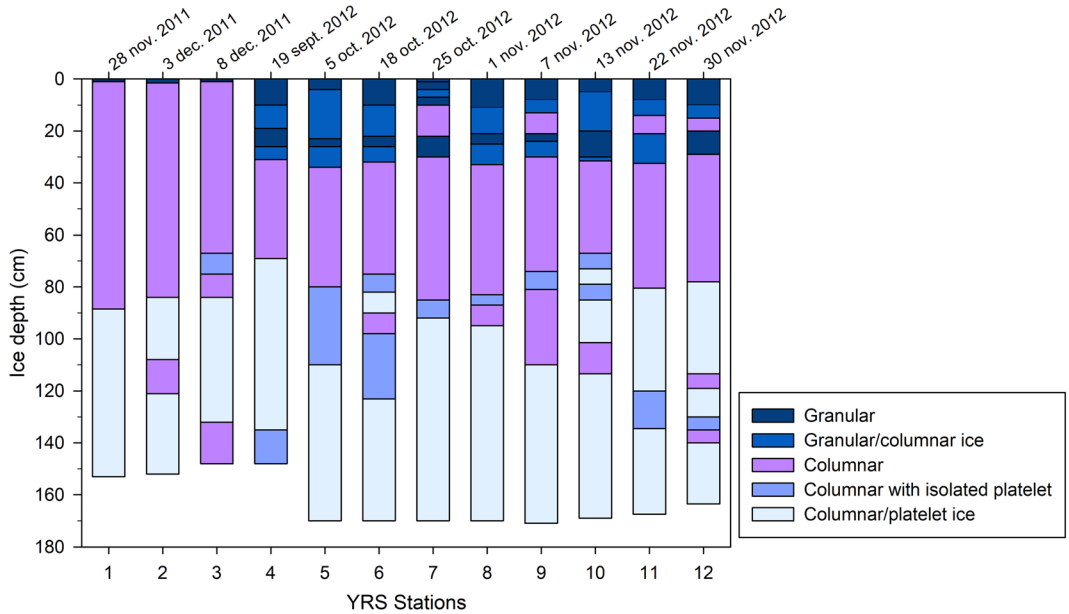

Figure 2. Ice texture of Yrosiae (YRS) stations from 2011 to 2012.

measurements were performed using the same 5 cm vertical resolution as for temperature measurements using a Thermo Scientific Orion® 3 Star conductivity meter (accuracy of 0.1‰). The conductivity meter was calibrated at the beginning and at the end of the survey with standard solutions (UNESCO, 1966). The conversion from conductivity to salinity is performed via a built-in temperature-dependent conversion program. Further details about physical measurements are provided in Carnat et al. (2013, 2014).

2.2.2. Air-Snow-Ice CO_2 Fluxes

CO_2 fluxes were measured using a LI-COR® LI-8100A soil CO_2 flux system. During the survey, two chambers were used and installed on the snow or on the ice after removing the initial snow cover. The chambers consist of a metal cylinder, with a diameter of 20 cm and a height of 9.7 cm, closed at the top by a mobile cap to vent the chamber and maintain an ambient pressure inside. A rubber seal surrounds the cylinder and ensures an airtight connection at the chamber-ice interface. For measurements over snow, a stainless steel seal was mounted at the base of the chamber and pushed down to the ice to enclose snow and prevent lateral diffusion of air in the snowpack.

The chambers (LI-COR® 8100-104) were temporarily closed above the snow or ice interface and were connected using a LI-COR® LI-8150 Multiplexer to an infrared gas analyzer LI-COR® LI-8100A recording the pCO_2 during a designated time interval (30 min). The flux was determined by measuring the change of pCO_2 within the chamber. Flux calculations were performed routinely using the LI-COR® SoilFluxPro software, with volumes adjusted to include collar offsets (i.e., rim height above the surface) and applying water vapor corrections for dilution and band broadening. The fluxes were determined by the slope of the linear or exponential regression of pCO_2 over time, depending on the best fit. All fluxes were visually checked to discard measurements biased by contamination or poor sealing of the chamber. The detection limit was ± 0.004 μmol m^{-2} s^{-1}. Fluxes below the detection limit were considered as null. The uncertainty of the flux computation due to the standard error of the regression slope was ±8%.

Table 1
Mean Snow Depths

Station	Sampling date	Mean snow depth (cm)
YRS1	28 November 2011	2.5
YRS2	3 December 2011	1.6
YRS3	8 December 2011	0.9
YRS4	19 September 2012	1.2
YRS5	5 October 2012	1.5
YRS6	18 October 2012	0.8
YRS7	25 October 2012	0.8
YRS8	1 November 2012	0.6
YRS9	7 November 2012	0.8
YRS10	13 November 2012	0.8
YRS11	22 November 2012	0.7
YRS12	30 November 2012	0

2.2.3. Thin Sections of Ice

Thin sections of thickness ranging from 600 to700 μm were obtained using a Leica SM2400 microtome. These thin sections were then examined on a light table equipped with cross-polarized sheets (Langway, 1958). The

textural types were visually identified based on the size, shape, and orientation of the ice crystals and compared to descriptions found in the literature (Eicken & Lange, 1991; Tison et al., 2013).

2.2.4. Biomass and Nutrients

One core per station was dedicated to chl-*a*, nutrients, and POC analyses. For chl-*a* analyses, ice sections of 10 cm were cut with a band saw, in the cold lab (at -25°C) on the day of extraction and subsequently melted at 4°C in the dark, in pre-filtered seawater. Melted ice was filtered using 10 μm and then 0.8 μm Nuclepore® polycarbonate membranes. Filters were stored frozen in cryovials until measurements at the home laboratory. Extraction was performed in 10 ml acetone at 4°C for 16 hr. Chl-*a* concentrations were determined using a Turner Design TD700 fluorometer.

Particulate organic carbon (POC) and nutrient analyses were performed at a 10 cm depth resolution for the bottom of the core, and at 30 cm resolution for the rest of the core. Samples were melted at room temperature in the dark and then filtered on 0.7 μm precombusted (5 hr at 450°C) GF/F filters (Whatman®). The filtrate was collected and stored in 60 ml acid-washed, pre-rinsed HDPE bottles. Both filters and filtrate were stored at −25°C. For POC analysis, filters were acid fumed (HCl) to remove carbonates and packed in silver cups fitting the autosampler. POC concentrations were determined using an Elemental analyzer (Eurovector®) coupled with an isotope ratio mass spectrometer (Delta V, Thermo®).

Nitrate plus nitrite ($[NO_3^-] + [NO_2^-]$), nitrite ($[NO_2^-]$), and phosphate ($[PO_4^{3-}]$) concentrations from filtered water samples were measured spectroscopically using a colorimetric method and a QuAAtro39 auto-analyzer (Seal Analytical Inc., Mequon, WI, USA).

The change over time of the nitrate plus nitrite concentrations was obtained from the following equation:

$$\Delta\left[NO_3^-\right] + \Delta\left[NO_2^-\right] = \frac{\left[NO_3^-\right](t_{n+1}) + \left[NO_2^-\right](t_{n+1}) - \left[NO_3^-\right](t_n) - \left[NO_2^-\right](t_n)}{\Delta t}\ \left(\mu\text{mol L}^{-1}\text{day}^{-1}\right) \quad (1)$$

Δt denotes the elapsed time between two stations, and t_n and t_{n+1} correspond to one station n and the next station ($n + 1$), respectively. The change over time of the POC concentrations was computed in the same way.

2.2.5. Total Alkalinity and pH

Ice cores were cut into 10 cm sections in a cold room (at −25°C). Each section was placed in a gas-tight Supelco® Tedlar® bag equipped with a push/pull lock valve. The bag was sealed with a clip, and the air was removed using a vacuum pump through the valve. The bagged sea ice samples were then melted at room temperature for less than 24 hr. Attention was paid to mix the bags regularly in order to keep the meltwater at melting temperature and to treat meltwater as soon as possible after complete melting to avoid warming of the meltwater and subsequent carbonate dissolution as suggested by Dieckmann et al. (2008). Meltwater was shaken to resuspend the crystals, and aliquots were collected for pH, bulk alkalinity (TAb), and filtered alkalinity (TAf) analyses. pH was measured using a Metrohm® combined electrode calibrated on the total hydrogen ion scale using TRIS (2-amino-2-hydroxymethyl-1.3-propanediol) and AMP (2-aminopyridine) buffers prepared at salinities of 5, 35, and 75 according to the formulations proposed by DOE (1994). The pH measurements were carried out at low temperature (typically below +4°C). The accuracy of pH measurements was ±0.01 pH units. Samples for TAf were filtered on 0.2 μm polycarbonate filters. Filtration was carried out at 4°C in order to avoid any dissolution of calcium carbonate. TA was measured by open-cell titration with HCl 0.1 M on 50 ml of sea ice melt samples, following Gran (1952) endpoint determination. Titration was stopped for 10 min at pH 4.2 to ensure the dissolution of any calcium carbonate crystals, prior to perform the measurements between pH of 4.2 and 3 required for the Gran function. The accuracy of TA measurements was ±4 μmol kg^{-1}. Data were quality checked with certified reference material from Andrew Dickson (Scripps Institution of Oceanography, University of California, San Diego).

2.2.6. O_2 and Ar Concentrations

The dry-crushing technique, developed for gas measurements in continental ice (Raynaud et al., 1982), was used to extract O_2 and Ar from the ice samples. This technique allows the extraction of both gas bubbles and gas dissolved in liquid brines. The ice core was cut into 5 cm sections, and each ice cube of about 60 g was placed into a vessel, with seven stainless steel balls. The latter was crushed in the vessel as described in Stefels et al. (2012), at a temperature of −25°C and under a vacuum of 10^{-3} Torr. The vessel was then kept at −50°C in a cold ethanol bath and connected to the gas chromatograph equipped with a thermal

conductivity detector for concentration analyses. We used He (Air Liquide®-Alphagaz 2) as the carrier gas and a 22 ml packed column (Mole Sieve 5A 80/100; 5 m × 1/8 in.). The repeatability of the analyses (i.e., the precision of the gas chromatograph) was 0.7% for O_2 and 2.2% for Ar (Zhou et al., 2014).

2.2.7. Bulk Ice pCO_2 Measurements

Bulk ice pCO_2 was measured using the method developed by Verbeke (2005) and Geilfus et al. (2012) and adapted by Crabeck et al. (2014). The general principle of the method is to equilibrate sea ice samples with a N_2/CO_2 gas mixture of known concentration (standard gas) as close as possible to the in situ temperature (i.e., the temperature of the ice upon ice collection). Once the ice sample is equilibrated, the gas phase is injected into a gas chromatograph (Varian 3300) to measure the CO_2 concentration (Geilfus, Carnat, et al., 2012).

The ice core was first cut with a vertical resolution of 5 cm. Ice sections were then precisely cut into 4 × 4 × 4.5 cm of cubes to tightly fit the equilibration container. Attention was paid to maximize the sea ice volume, to minimize the headspace volume, and to keep it equivalent for each sample. Standard gas was injected at atmospheric pressure into the headspace of the container containing the ice sample. Tests were carried out with standard gas at 150, 300, and 500 ppm. While the three standards gave consistent results below 200 ppm, as expected the 150 ppm standard provided underestimated measurements above 200 ppm. Standards at 300 and 500 ppm provided consistent results below 350 ppm and above 500 ppm, and overestimated values in between were observed with the standard at 500 ppm. As a consequence, we used a standard gas of 300 ppm for all samples. The container, kept at −50°C during the standard injection, was then placed in a thermostatic bath to bring the ice sample to the in situ temperature. After 20 hr, the sample was assumed to be in equilibrium with the standard gas (Crabeck et al., 2014; Geilfus, Carnat, et al., 2012). The headspace was then injected in the gas chromatograph to measure the CO_2 concentration. Shortly afterward, the sample temperature was measured using a calibrated probe (TESTO® 720). The method is expected to be valid if the ice is permeable at the in situ conditions. Standard gas concentration should be as close as possible from the expected concentration of the sample in order to achieve sufficient accuracy (Verbeke, 2005).

The precision of the measurements was estimated based on 28 injections of standard gas 300 ppm (injection pressure ranged between 10 and 99 Torr). We obtained a mean relative error of 2.1%, a standard deviation of 9.8 ppm, and a variation coefficient of 3.3%.

2.3. Computed Parameters

2.3.1. Brine Volume and Rayleigh Number

The brine volume fraction (BrV), a proxy of sea ice permeability, was computed from ice temperature and salinity following the equations of Cox and Weeks (1983) for ice temperature <−2°C and Leppäranta and Manninen (1988) for ice temperature ≥−2°C. We considered that the ice was permeable for a brine volume fraction exceeding 5% (Golden et al., 1998). The Rayleigh number (Ra) was used as a proxy of the intensity of brine convection (Notz & Worster, 2008) which is driven by the density difference between high-salinity brine in sea ice and the seawater underneath (Vancoppenolle et al., 2013). Theoretically, convection can occur in an ice layer when Ra exceeds a critical value of 10 (Notz & Worster, 2008) or 7.5 (Zhou et al., 2013) according to experimental studies. The critical value could also be considered as low as 4 (Carnat et al., 2013; Vancoppenolle et al., 2013) although this critical value is still quite debated and also sensitive to the potential delay between occurrence and observation.

2.3.2. DIC

Dissolved inorganic carbon (DIC) was computed from TAf and pH (presented in Figure S1), according to CO_2 acidity constants of Goyet and Poisson (1989) as suggested by Brown et al. (2014) for measurement in brines at subzero temperatures, and other constants proposed by DOE (1994). We used TAf for DIC computation in order to avoid bias from the potential dissolution of particulate inorganic carbon (e.g., ikaite formed in sea ice).

DIC and TAf were normalized to a salinity of 6, the mean bulk ice salinity, in order to remove the salinity-related changes (i.e., brine rejection, concentration, and dilution). The normalized DIC and TAf are referenced hereafter as DIC_6 and TAf_6, respectively.

2.3.3. NCP From DIC

Net community production based on inorganic carbon deficits (NCP_{DIC}) was computed from changes in observed DIC, TAf, nitrate plus nitrite, and phosphate according to

$$NCP_{DIC} = -\frac{\Delta DIC}{\Delta t} + 0.5\frac{\Delta TAf + \Delta NO_3^- + \Delta NO_2^- + \Delta PO_4^{3-}}{\Delta t} \quad (2)$$

where Δt denotes elapsed time between two stations (Delille et al., 2005). The second term of the Equation 2 corresponds to the difference in carbonate alkalinity due to the formation or dissolution of calcium carbonate. ΔDIC is the difference between DIC(t_{n+1}) and DIC (t_n) normalized to the S(t_{n+1}), t_n and t_{n+1} corresponding to the station n and the next station (n + 1). ΔTAf, $\Delta NO_3^- + \Delta NO_2^-$ and ΔPO_4^{3-} were computed in the same way. We assumed that no physical process has affected the bulk impurity content of the ice from one station to the next one and that all these changes are therefore due to biological processes. NCP_{DIC} is given in mg C m^{-2} day^{-1}.

2.3.4. NCP From O_2/Ar Ratios

Oxygen concentrations in sea ice depend on both biological activity and physical processes. We used argon measurements to remove the influence of physical impact on O_2 concentrations. Argon has indeed no biological sources or sinks, but it is affected by physical processes in the same way as oxygen concentrations. O_2 concentrations associated to in situ biological activity ($[O_2]_{bio}$) were obtained from O_2/Ar ratios and their deviation from saturation as described for seawater by Reuer et al. (2007) and adapted for sea ice by Zhou et al. (2014).

O_2/Ar ratios observed in ice were compared with atmospheric and seawater ratios to determine the abiotic range of O_2/Ar values. Within the abiotic range of O_2/Ar values, it is not possible to discriminate biological processes from physicochemical processes, since changes of O_2/Ar ratio can be ascribed to biological processes but also to the input of atmospheric air or underlying seawater. The atmospheric O_2/Ar ratio is 22.5 based on O_2 and Ar mixing ratios in the atmosphere (NOAA, 1976). Any gas input from the atmosphere or gas bubble formation would push the bulk ice O_2/Ar ratio toward 22.5. At the seawater interface, considering conditions of −1.8°C and a salinity of 34, the O_2/Ar ratio is 20.5 (Garcia & Gordon, 1992; Hamme & Emerson, 2004). Given these ratios, the abiotic range of O_2/Ar in sea ice is determined to lie between 20.5 and 22.5. Out of this range, O_2/Ar values were attributed to the impact of biological activity only and have been considered for computation of net community production.

In order to do so, we first calculated the theoretical brine solubility of each gas using temperature, the salinity of the brine calculated from ice temperature (Cox & Weeks, 1986) and the relationships from Garcia and Gordon (1992) for O_2 and Hamme and Emerson (2004) for Ar. Brine solubility multiplied by the brine volume fraction gives the gas solubility in bulk ice (hereafter referred as $[O_2]_{eq}$ and $[Ar]_{eq}$).

The O_2/Ar deviation from saturation was calculated as follows:

$$\Delta(O_2/Ar) = \frac{[O_2]/[Ar]}{[O_2]_{eq}/[Ar]_{eq}} - 1 \quad (3)$$

$[O_2]$ and [Ar] are the sea ice concentrations measured at a vertical resolution of 5 cm and interpolated using the IDL program (Harris Geospatial). O_2 and Ar supersaturation are commonly observed in sea ice (Zhou et al., 2014), indicating that equilibrium concentrations can differ from their solubilities due to physical processes. In order to deal with potential biases while using O_2 and Ar solubilities for $[O_2]_{eq}$ and $[Ar]_{eq}$, we modified the calculations from Zhou et al. (2014) as follows:

$$[O_2]_{phy} = [O_2]_{eq}\left([Ar]/[Ar]_{eq}\right) \quad (4)$$

The O_2 concentration associated with in situ biological activity is then defined using the following equation:

$$[O_2]_{bio}=[O_2]_{phy}\,\Delta(O_2/Ar)\ (\mu mol\ L^{-1}) \tag{5}$$

The daily O_2 production is given in μmol L^{-1} day^{-1}. We considered the ice thickness, a O_2/C ratio of 1.43 (Glud et al., 2002) and the molar mass of C in order to derive the C uptake equivalent (mg C m^{-2} day^{-1}).

The propagation of uncertainties on $[O_2]_{bio}$ was estimated using a Monte Carlo approach. We neglected the error on gas diffusion assuming equivalent diffusivities for O_2 and Ar in sea ice as in Crabeck et al. (2014). Each parameter was given a distribution to represent its uncertainty sampled over 10^5 iterations. Normal or uniform distributions between the mean ± error of measurements were used. Measured parameters (T, S, O_2, and Ar) were given normal distribution with the mean population and an error of 0.2 for T, 0.1 for S, 0.7% for O_2, and 2.2% for Ar. The error on $[O_2]_{eq}/[Ar]_{eq}$ ratio is prone to larger uncertainties and was therefore given a uniform distribution of 9.9% either side of calculated value to account for gas bubble formation in sea ice (Zhou et al., 2014). The obtained maximum uncertainty of $[O_2]_{bio}$ was 19.6%.

Net community production (NCP) is determined from the change over time of oxygen concentrations associated to in situ biological activity ($[O_2]_{bio}$) as follows:

$$NCP=\frac{[O_2]_{bio}\ (t_{n+1})-[O_2]_{bio}\ (t_n)}{\Delta t}\ (\mu mol\ L^{-1} day^{-1}) \tag{6}$$

Δt denotes elapsed time between two stations, and t_n and t_{n+1} correspond to the station n and the next station $(n+1)$, respectively.

2.3.5. Assessment of Calcium Carbonate Content

Two different indicators were used to assess calcium carbonate precipitation: the overall $CaCO_3$ content ($[CaCO_3]$) and the saturation state of ikaite (Ω_{ika}).

The overall $CaCO_3$ content was estimated from the difference between total alkalinity of a nonfiltered sample, denoted as bulk alkalinity (TAb) and total alkalinity of the filtered sample, denoted as filtered alkalinity (TAf) (Geilfus et al., 2013), according to:

$$[CaCO_3]=\frac{1}{2}(TAb-TAf) \tag{7}$$

Calcium carbonate precipitation (dissolution) can take place if the saturation state of ikaite in brine $\Omega_{ika}>1$ ($\Omega_{ika}<1$). The saturation state of ikaite Ω_{ika} in brine depends on the concentrations of calcium and carbonate in brine and their solubility product described as a function of temperature T(K) by Papadimitriou et al. (2013):

$$pK_{sp,ikaite}=-15489.09608+623443.70216\ T^{-1}+2355.14596\ \ln T \tag{8}$$

While this solubility product has been established for temperatures above −8°C, we used it below this threshold and assumed it constant. We acknowledge that we neglected some physical processes such as concentration and dilution. This approach thus presents some limitations. We estimated the salinity of brines using a third-order fit from Assur (1958) and Notz (2005). We also computed TA_{brines} and DIC_{brines} by considering their linear dependence to salinity in order to obtain CO_3^{2-} brine concentrations from CO2SYS program for the carbonate system (Lewis et al., 1998). More details can be found in Moreau et al. (2015).

3. Results

3.1. Sea Ice and Snow Properties

Main sampling took place from late winter (September 2012), when daylight was still short and the air temperature was low (down to −32°C), to late spring (November 2012). Three stations were also carried out in November-December 2011 with an air temperature above -6°C and high solar irradiance (Figure 3). The mean sea ice thickness ranged between 145 and 171.4 cm (Figure 2). The ice texture was homogenous between stations. From top to bottom, we observed a thin layer of granular ice followed by a mixture of granular and columnar ice, a thick layer of columnar ice, columnar ice with isolated platelets, and a bottom layer

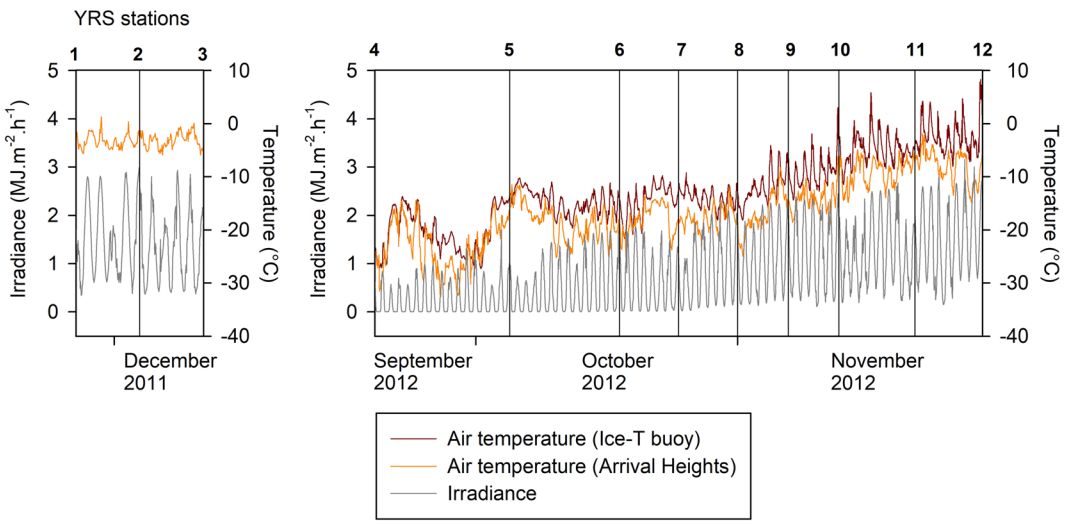

Figure 3. Evolution of air temperature recorded by the ce-T buoy in 2012 (brown line), air temperature (orange line), and solar radiation (gray line) in 2011 and 2012 recorded by the weather station at Arrival Heights (23 km away from sampling location).

of columnar and platelet ice (Figure 2). The snow cover ranged from 0 to 4 cm thick, with salinities ranging from 7.4 to 24.5.

The bulk ice temperature ranged from −19.8°C to −0.8°C and showed a strong vertical gradient (Figure 4a). The lowest ice temperature appeared in the upper layer in winter while the temperature in bottom ice was close to the freezing point (i.e., −1.8°C). At the end of the spring (stations YRS1 to YRS3), the ice displayed a nearly isothermal profile. As the ice temperature increased in spring, the ice became fully permeable from station YRS10 (Figure 4c), when the brine volume fraction exceeded 5%, the threshold for fluid transport (Golden et al., 1998).

The vertical distribution of salinity showed little changes from YRS4 to YRS10 after which surface salinity decreased (Figure 4b). Homogenous salinity profiles were observed in late spring 2012 (stations YRS11 and YRS12) and 2011 (stations YRS1-YRS3). The average bulk salinity for the whole data set was 6. The Rayleigh (Ra) number started to increase at station YRS7 and reached a maximal value of 17 at station YRS11, exceeding the critical convection threshold of 10 (Notz & Worster, 2008). Ra values indicated a convective event in station YRS11 (Figure 4d). However, apart from this specific event, Ra values did not indicate any other obvious convective event, consistently with the salinity distribution.

3.2. Ice Carbon Content

3.2.1. A "Three-Layers" Model Based on DIC_6

DIC_6 ranged from 194 to 563 μmol kg^{-1} (Figure 5b) and exhibited strong vertical gradients within the ice column. These gradients were used to discriminate the ice column in three layers: surface, interior, and bottom. The layer between 20% and 83% of the ice thickness is considered as the interior layer and corresponds to relatively constant (standard deviation below 69 μmol kg^{-1}) and highest DIC_6 values (except in late spring from stations YRS1 to YRS3). The surface and bottom layers account for 20% and 17% of the total ice column, respectively (Figure 5b).

DIC_6 increased at all depths from stations YRS4 to YRS6 and then rapidly decreased between stations YRS6 and YRS7. From station YRS7 onwards, DIC_6 values in the surface and bottom layers significantly deviate compared to the mean value observed in the ice interior. Surface DIC_6 oscillated with both increasing and decreasing periods while bottom DIC_6 remained low (<352 μmol kg^{-1} except for station YRS11) and below seawater values (mean DIC_{SW} normalized to salinity 6: 378.8 ± 17.3 μmol kg^{-1} at 0 m depth), although slightly increasing at the end of the study (YRS11 and YRS12).

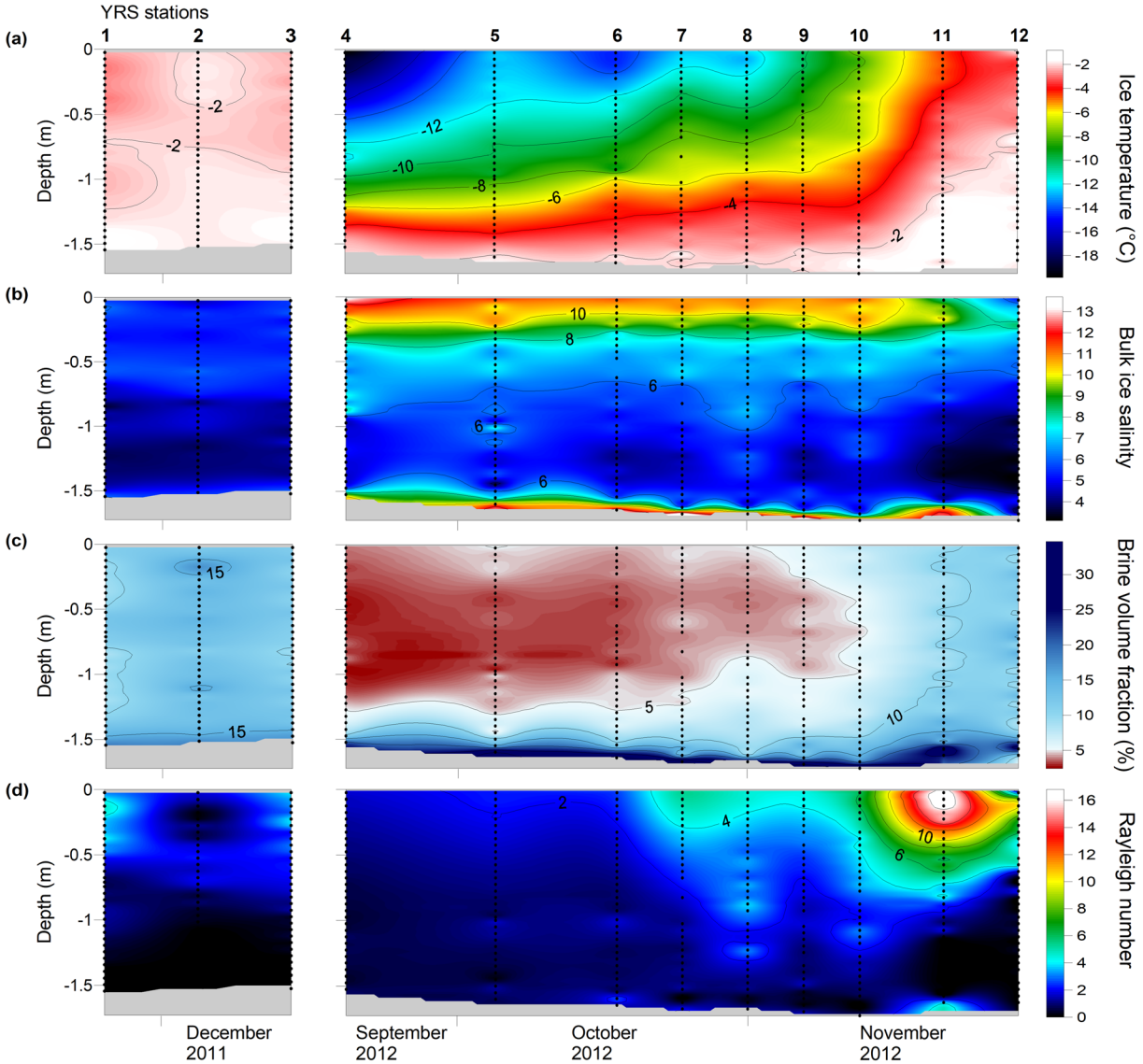

Figure 4. Temporal evolution of (a) ice temperature, (b) bulk ice salinity, (c) brine volume fraction, and (d) Rayleigh number. Plots were produced using the radial basis function method for interpolation in Surfer 8 software. Black dots are data points from field sampling.

Changes in DIC_6 are mainly due to biogeochemical processes such as CO_2 consumption or production, precipitation, and dissolution of calcium carbonate and exchanges of $CO_{2(g)}$.

3.2.2. Calcium Carbonate Precipitation

TAf_6 increased gradually at the bottom of the ice during spring, from station YRS7 to station YRS12, reaching values up to 550 μmol kg^{-1} (Figure 5a). The $CaCO_3$ content followed the same trend as TAf_6 at the bottom of the ice suggesting localized calcium carbonate precipitation. We estimated that up to 350 μmol kg^{-1} $CaCO_3$ precipitated in late spring (Figure 5c). Accordingly, high Ω_{ika} values were mainly observed at the bottom of the ice from stations YRS7 to YRS12 (Figure 5d). At the sea ice surface, no significant calcium carbonate precipitation occurred at the sea ice surface except potentially at stations YRS11 and YRS12.

3.3. Biomass and Nitrate Concentrations

Most of the ice algal biomass (66% to 99.9%) was concentrated in the bottom 10 cm of the ice (Table S2) with values reaching over 2,400 μg L^{-1} in spring (Figure 6a). Under-ice seawater concentrations remained low

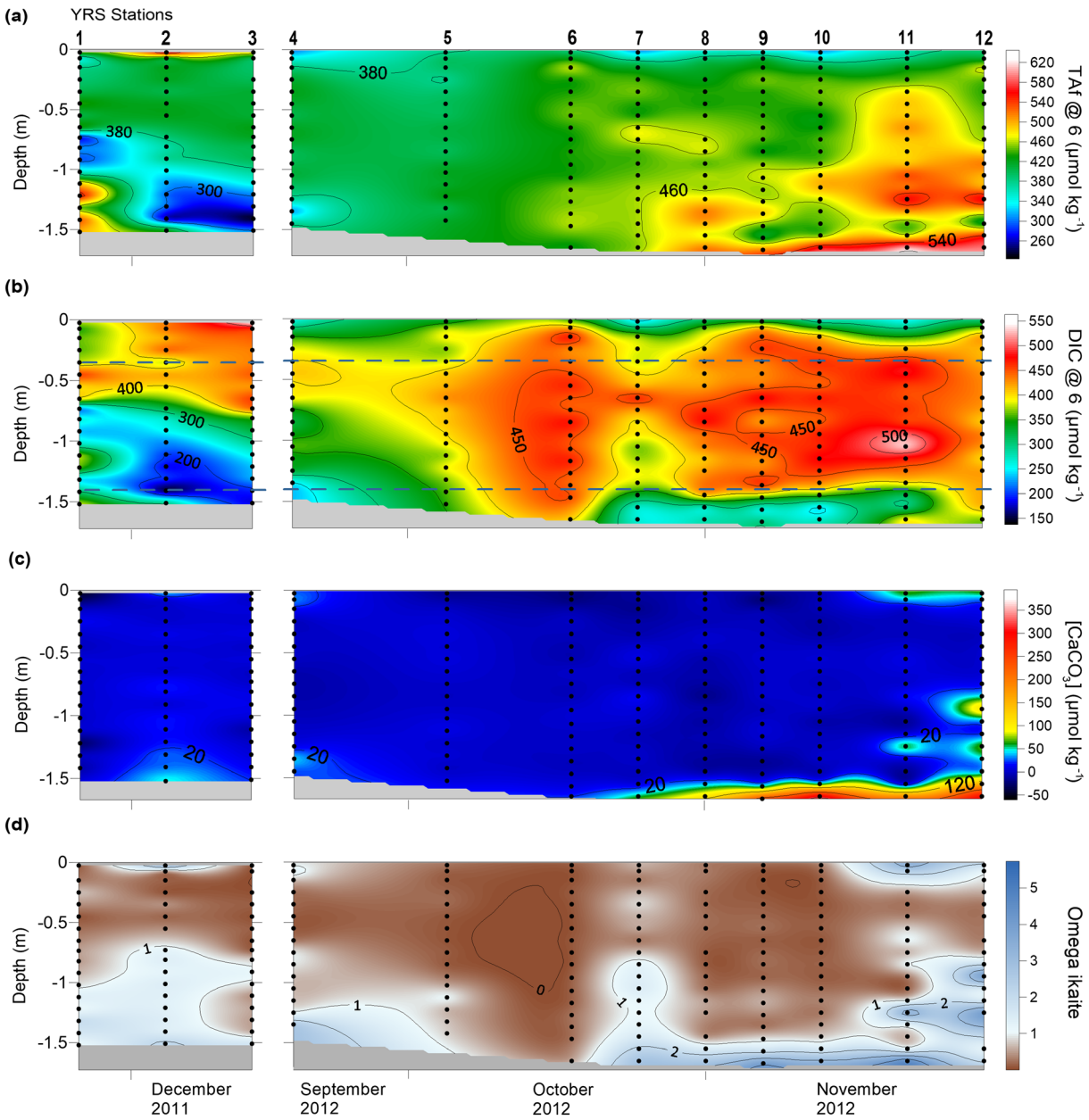

Figure 5. Temporal evolution of (a) TAf_6, (b) DIC_6, (c) $CaCO_3$ content, and (d) omega ikaite. Black dots are data points from field sampling. Horizontal blue lines mark the limits between the surface, interior, and bottom layers of the ice. Plots were produced using the radial basis function method for interpolation in Surfer 8 software.

(<0.41 $\mu g\ L^{-1}$) from stations YRS4 to YRS12. The onset of the spring ice algal bloom was initiated at YRS6 and chl-*a* was accumulating until station YRS10.

POC accumulated in parallel with the increasing algal biomass in the bottom ice. POC concentrations increased by 1,100 $\mu mol\ L^{-1}$ between stations YRS8 and YRS10 (in 12 days) to reach maximum value around 2,600 $\mu mol\ L^{-1}$ in station YRS10 (Figure 6b). Bulk concentrations of nitrate plus nitrite ranged from 0.1 to 97.1 $\mu mol\ L^{-1}$ (Figure S2). Changes over time of nitrate plus nitrite concentrations and POC concentrations, calculated using Equation 1, are shown in the Figures 7a and 7b. Positive values indicate an increase between the two stations considered while negative values indicate a decrease. Both nitrate plus nitrite and POC concentrations were higher in absolute value at the bottom of the ice than in the ice interior

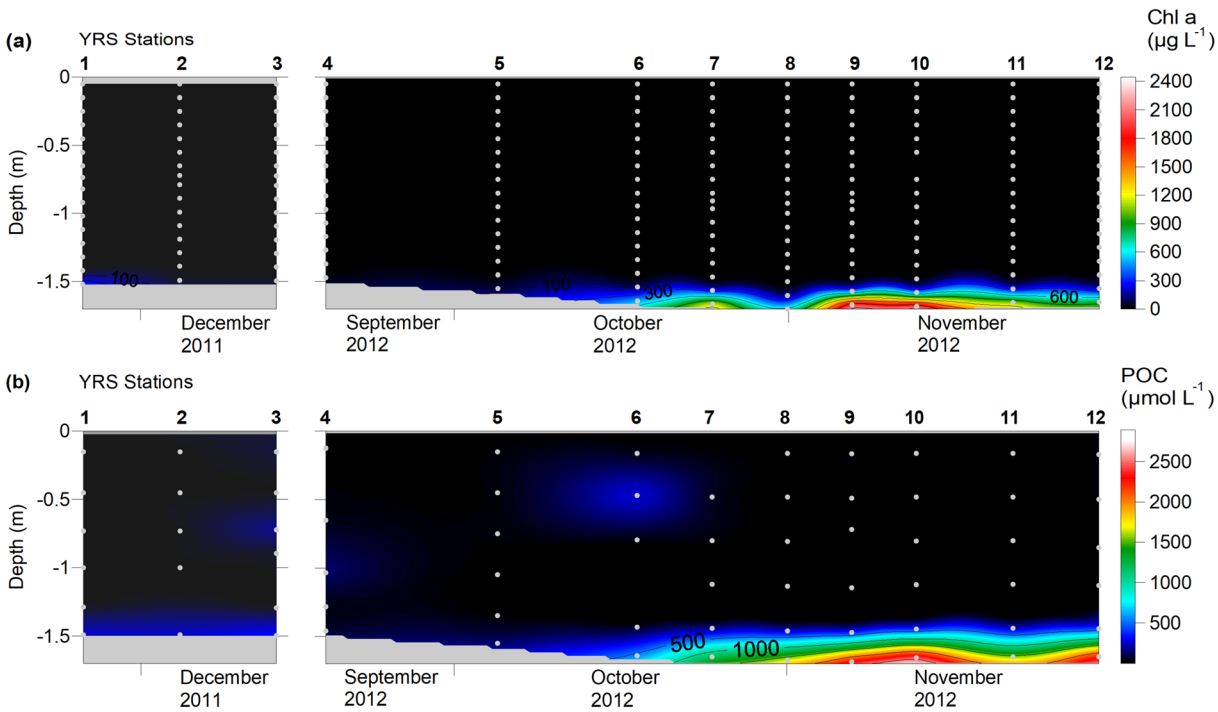

Figure 6. Temporal evolution of (a) chlorophyll *a* and (b) POC concentrations in sea ice. Plots were produced using the radial basis function method for interpolation in Surfer 8 software. Gray dots are data points from field sampling.

and at the surface. Bottom concentrations increased between each station until YRS10 before collapsing at station YRS11.

3.4. Oxygen Concentrations

The O_2 and O_2bio concentrations ranged from 14 to 272 μmol L^{-1} and −13 to 206 μmol L^{-1}, respectively (Figures 8a and 8b). The maximum concentrations of O_2 and O_2bio were encountered in the bottom sea ice where maximum values of chl-*a* were observed. An increase in oxygen concentrations was observed from YRS4 to YRS8 during the exponential phase of the bloom and a decrease occurred afterward. Our data highlighted a major biogenic contribution to the molecular oxygen pool: O_2bio concentrations accounted for 60% to 80% of the O_2 pool at the bottom (Figure 8c).

3.5. NCP

Figure 7 presents the variables used as tracers of production during this study, which have been computed consistently (i.e., same depths and time steps). Tracers of production are changes in nitrate plus nitrite (in μmol L^{-1} day^{-1}, Figure 7a), POC (in μmol L^{-1} day^{-1}, Figure 7b), NCP derived from O_2/A ratios ($NCP_{O2:Ar}$ in μmol L^{-1} day^{-1}, Figure 7c), and NCP derived from DIC (NCP_{DIC} in mg C m^{-2} day^{-1}, Figure 7e). These assessments are given for each layer (surface, interior, and bottom) with the exception of NCP_{DIC} given only for the interior ice. While $NCP_{O2:Ar}$ accounts for gas exchanges thanks to the use of Ar concentrations to trace physical processes, NCP_{DIC} is sensitive to CO_2 fluxes at the interfaces-surface and bottom layers-preventing robust estimates in theses layers. In order to allow comparison with the literature, we also provided integrated $NCP_{O2:Ar}$ (mg C m^{-2} day^{-1}) for the entire ice column (Figure 7d).

Bottom $NCP_{O2:Ar}$ ranged between −4.3 to 3.8 μmol L^{-1} day^{-1}. Positive NCP indicates an oxygen production (equivalent to an inorganic carbon uptake) while negative NCP corresponds to oxygen consumption (equivalent to inorganic carbon production). We compared our measurements with available data of net community production in Arctic sea ice (Table 2). Our measurements fall within the estimates carried out either by O_2/Ar assessment or oxygen incubation. Our values are at the lower end of previous estimates of

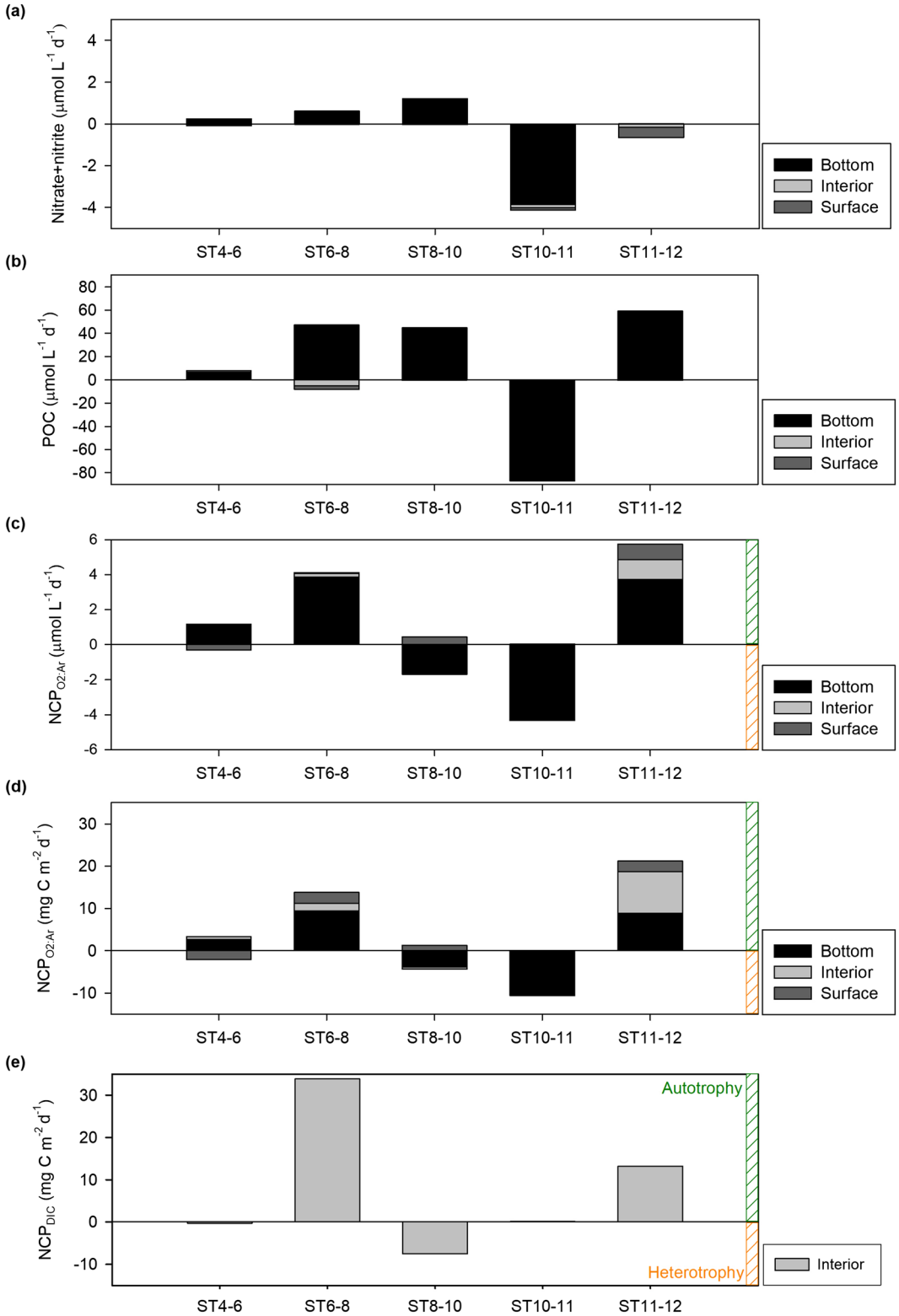

Figure 7. Temporal changes of (a) nitrate plus nitrite concentrations and (b) POC concentrations in surface, bottom, and interior ice layers. Net community production derived from (c, d) O_2/Ar and (e) DIC.

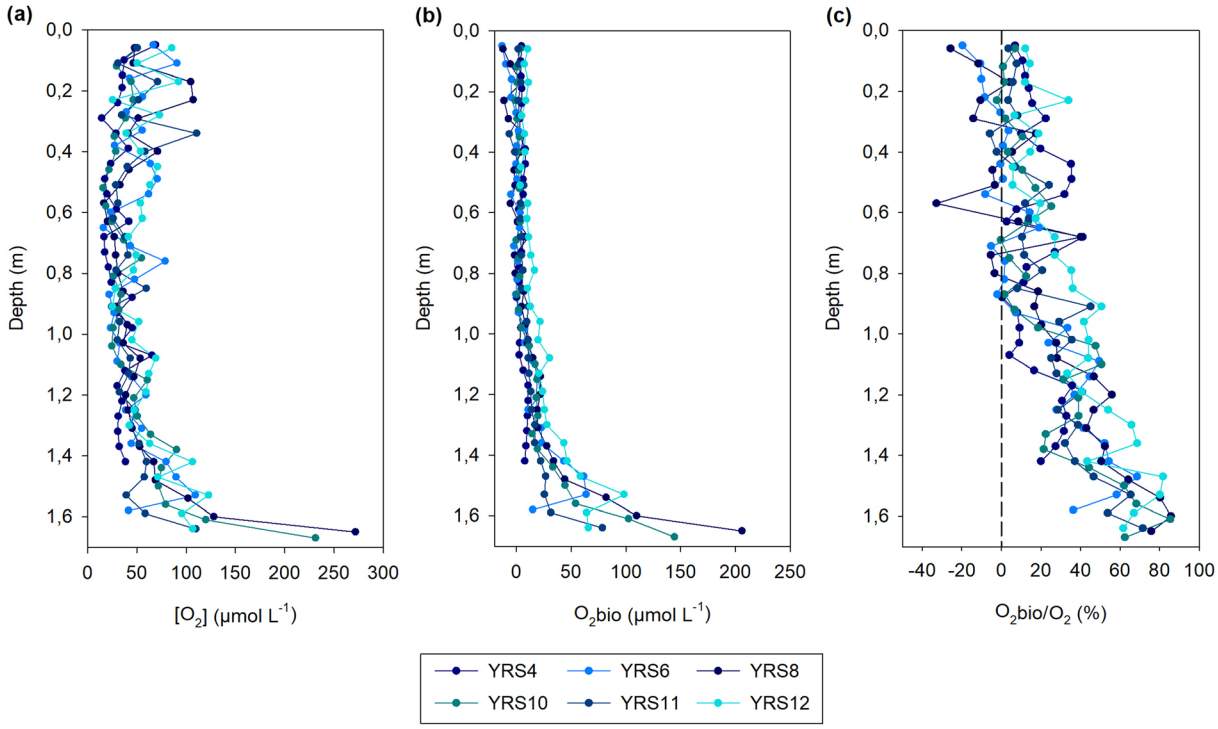

Figure 8. Vertical profiles of (a) O_2 concentrations in bulk ice, (b) $[O_2]_{bio}$ calculated from Equation 5, and (c) O_2bio/O_2 ratio.

NCP for bottom Antarctic sea ice from McMinn et al. (2012) derived from in situ oxygen fluxes across the downward boundary layer estimated with an oxygen microelectrode.

$NCP_{O2:Ar}$ was higher in absolute value in the bottom sea ice compared to the upper layers (Figure 7c). At the bottom, NCP was positive at the end of the winter indicating a net autotrophy (stations YRS4–YRS8), then heterotrophy dominated during spring (YRS8–YRS11) before it turned back to autotrophy at the end of the spring (YRS11 and YRS12). In the ice interior, the same pattern was observed, although with a lower amplitude. Autotrophy dominated the sea ice surface except from stations YRS4 to YRS6.

We compared $NCP_{O2:Ar}$ with NCP_{DIC} for the interior ice. NCP_{DIC} showed similar trends and the same order of magnitude as $NCP_{O2:Ar}$ for stations YRS8–YRS10 and YRS11–YRS12. A discrepancy in terms of magnitude appeared for stations YRS6–YRS8.

Table 2
Community Production Rates for Landfast Sea Ice of the Arctic and Southern Oceans

Location	Layer	Method	NCP (µmol L^{-1} day^{-1})	NCP (mg C m^{-2} day^{-1})	References
Arctic Ocean					
Barrow, Alaska	Surface -internal	O_2/Ar	−6.6–3.6	—	Zhou et al. (2014)
Malene Bight, SW Greenland	Surface	Oxygen incubations	0.8 ± 3.5	—	Søgaard et al. (2010)
	bottom		6.3 ± 2.3	—	
Nunavut, Canada	Bottom	Oxygen optode incubations	1.6–2.8	—	Campbell et al. (2017)
Southern Ocean					
McMurdo Sound	Bottom	O_2/Ar	−4.3–3.8	−10.6–9.3	This study
McMurdo Sound	Bottom, platelet	Standing crop of chl-*a*	—	170–1,200	Arrigo et al. (1995)
Casey Station (East Antarctica)	Bottom	O_2 microelectrode	—	103–163	McMinn et al. (2012)
McMurdo Sound	Internal	O_2/Ar	−0.1–1.1	−0.5–9.8	This study
	Surface		−0.3–0.9	−2–2.6	

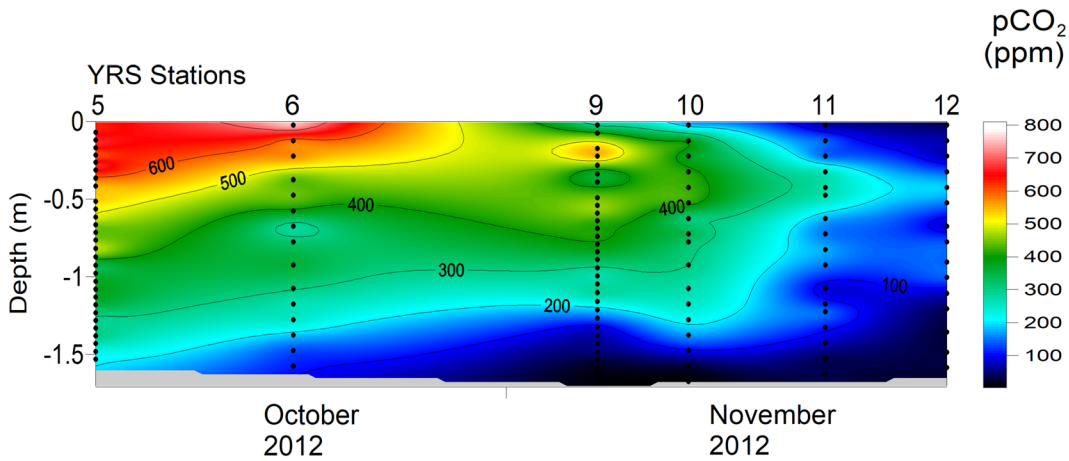

Figure 9. Temporal evolution of pCO_2. Samples were analyzed with a standard gas of 300 ppm. Black dots are data points from field sampling. This plot was produced using the radial basis function method for interpolation in Surfer 8 software.

3.6. pCO_2

The sea ice pCO_2 ranged from 2 to 810 ppm during the survey (Figure 9). The strongest pCO_2 gradient throughout the ice column was observed at YRS6, where the pCO_2 increased from 120 ppm at the bottom to 810 ppm at the top of the ice core. In late winter, pCO_2 undersaturation relative to the atmosphere was observed at the bottom of the ice with pCO_2 increasing towards the ice surface where oversaturation conditions prevailed.

The upper 10 cm of sea ice became undersaturated at station YRS9 with surface pCO_2 as low as 230 ppm. From station YRS10, the pCO_2 decreased throughout the ice column with particularly low pCO_2 at the surface (<45 ppm) for stations YRS11 and YRS12. The YRS3 profile obtained the previous year at a similar stage of the ice melting season showed a similar trend (Figure S3). The entire ice column was undersaturated in late spring.

Bottom pCO_2 remained particularly low during the entire study period (below 210 ppm or even below 40 ppm for stations YRS11, YRS12, and YRS3).

The pCO_2 values observed in this study fall within the same range of previous sea ice measurements in the Southern Ocean (Delille et al., 2014; Geilfus et al., 2014) despite the fact that the measurement methods differ (bulk vs. brines). All the studies reported in Table 3 showed recurrent low pCO_2 values observed in the ice and brines.

3.7. Air-Snow-Ice CO_2 Fluxes

The CO_2 fluxes measured over bare sea ice and snow ranged from −2.51 to 1.81 mmol m^{-2} day^{-1}, and from −9.76 to 6.22 mmol m^{-2} day^{-1}, respectively. In late winter and early spring (September–October), fluxes at the snow-air interface generally exceeded fluxes over bare ice (Figure 10). In late spring (end of November), both negative and positive fluxes occurred over 24-hr periods (Figure 11).

Data were slightly higher than values previously reported in Antarctica at the same season and using the chamber technique, although falling within the same order of magnitude (Table S1). Available data showed that both negative and positive fluxes are observed during spring in polar regions.

4. Discussion

4.1. The Bottom: Biofilm Implication

4.1.1. The High TAf—High Ω_{ika} Conundrum

The most striking feature of TAf_6 is the increase in the bottom layers at the end of the spring 2012 (Figure 5a). The dissolution of calcium carbonate crystals (e.g., ikaite) would have increased the TAf_6.

Table 3
Summarized Data for Bulk and Brine pCO_2 Records in the Arctic and Southern Oceans as well as in Saroma-Ko

Location	Ice type	Method	Season	pCO_2 (ppm)	References
Saroma-Ko, Japan	Landfast ice	Computed from brine DIC/TA	Winter	2.7–195	Nomura, Yoshikawa-Inoue, et al. (2010)
Arctic Ocean					
Resolute Passage, Nunavut	Landfast ice (first year)	Computed from brine DIC/TA	Spring	200–1,128	Brown et al. (2015)
		Brine pCO_2 computed from bulk DIC/TA		2–3,326	
		In situ brine (peepers)		230–1,280	
Resolute Passage, Nunavut	Landfast ice (first year)	In situ bulk	Late Spring	6–182	Geilfus et al. (2015)
		Bulk computed from DIC/TA		0–32	
		In situ brine		20–389	
Point Barrow, Alaska	Landfast ice (first year)	In situ bulk	Spring	23–442	Geilfus, Carnat, et al. (2012)
Amundsen Gulf, Beaufort Sea	Pack ice and landfast ice	In situ brine	Spring	0–1,839	Geilfus, Delille, et al. (2012)
Nuuk, Greenland	Landfast ice	In situ bulk	Spring	77–330	Crabeck et al. (2014)
Southern Ocean					
Bellingshausen Sea	Pack ice (first year)	In situ bulk	Spring	9–193	Geilfus et al. (2014)
Bellingshausen Sea, Weddell Sea, Indian sector of the SO	Pack ice (first year)	In situ brine	Spring-summer	28–921	Delille et al. (2014)
Cape Evans (Ross Sea)	Landfast ice	In situ bulk	Spring-summer	2–810	This study

However, this increase in TAf_6 co-occurred with calcium carbonate precipitation supported by high Ω_{ika} and high estimated $CaCO_3$ content at the bottom of the ice (Figures 5c and 5d). We find the origin of this particulate inorganic carbon to be puzzling since inorganic calcium carbonate precipitation or any biogenic calcification (i.e., colonization by planktic foraminifera) would decrease TAf_6 in a closed system, which is opposite to our observations. This implies that excess TAf_6 must have a different origin.

This accumulation of TAf_6 mimics the increase of nutrients at the bottom of the ice during the survey (Figure S2) that has been ascribed to the development of a biofilm (Roukaerts, 2018). Ice-associated biofilms have been suggested in several studies (Boetius et al., 2015; Deming, 2010; Meiners et al., 2003, 2008). Extracellular polysaccharide substances (EPS) secreted by bacteria and algae in sea ice (Krembs & Engel, 2001; Meiners et al., 2003, 2008; Riedel et al., 2006, 2007) are forming a gelatinous network (Decho, 2000; Decho & Gutierrez, 2017; Stewart & Franklin, 2008) and are therefore the backbone of the biofilm. Roukaerts (2018) showed that the development of a biofilm could drive the accumulation of nutrients at the bottom of the ice. In the same way, nutrient trapping was suggested as one of the functions of EPS aggregates and associated biofilm by Stewart and Franklin (2008). Biofilm microenvironments host intense remineralization of organic matter and allow accumulation of nutrients due to the relatively slow diffusion of dissolved compounds between the static biofilm and flowing brine (Stewart, 2003; Stewart & Franklin, 2008). We surmise that the increase in TAf_6 is partly due to the same process or accumulation of dissolved compounds in the biofilm. Besides promoting the storage of calcium carbonate, the presence of the biofilm might also trigger its precipitation. EPS functional groups, mainly negatively charged, can bind to substantial amounts of free Ca^{2+} or other metals (Braissant et al., 2007). This calcium-binding property may initially inhibit calcium carbonate precipitation, but subsequent sequential EPS degradation can create nucleation sites and foster calcium carbonate precipitation (Braissant et al., 2009). The authors developed a conceptual model of microbially mediated calcium carbonate precipitation in the EPS matrix (Figure 12). In the first two steps, the calcium binds to various EPS chemical functional groups (i.e., carboxyl, phosphate, amine, and sulfate esters). This EPS-Ca binding form a complex with a low-molecular-weight (LMW) organic carbon compound. Upon microbial enzymatic activity, the LMW organic carbon compounds are released and oxidized to bicarbonate, which in turn increases the alkalinity inside the

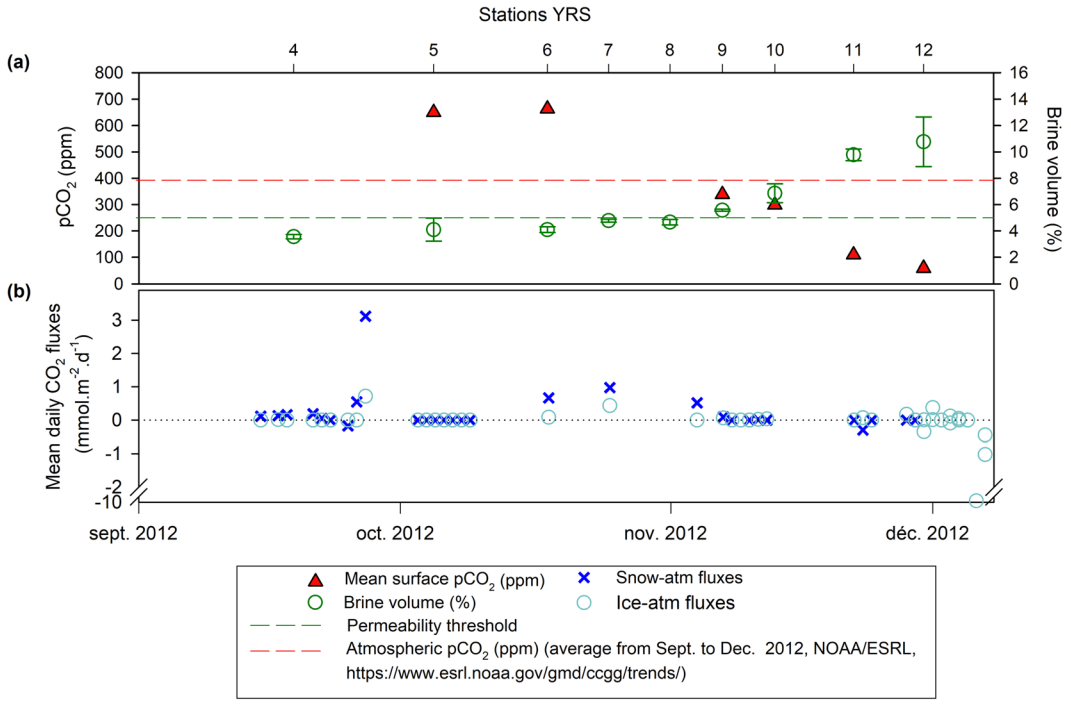

Figure 10. Temporal evolution of (a) mean pCO_2 (ppm, red symbols, left axis) for the top 15 cm of the and the corresponding mean BrV (%, green symbols, right axis) (b) daily mean CO_2 fluxes (mmol m^{-2} d^{-1}) over the ice (light blue open circles) and the snow (dark blue crosses). Positive values indicate CO_2 release to the atmosphere, and negative values indicate CO_2 uptake.

biofilm. Enzymatic activity in sea ice is supported by the presence of cold-active extracellular enzymes able to drive enzymatic hydrolysis or breakdown (Deming, 2007; Helmke & Weyland, 1995; Huston et al., 2000). Finally, the remaining free EPS-Ca sites allow for calcium carbonate precipitation within the EPS matrix. Calcium carbonate precipitation can thus occur in parallel with an increase of alkalinity within the biofilm at the bottom of sea ice, as nitrate plus nitrite concentrations increase in parallel with organic carbon production.

4.1.2. NCP as an Indicator of Trophic Status

The contribution of $O_{2\ bio}$ to the oxygen pool in sea ice increases steadily with depth (Figure 8c). Besides the impact of physical processes (e.g., solubility changes, brine concentration or dilution, and vertical transport), biological processes account for up to 80% of the overall oxygen content of the sea ice. The maximal contribution is observed at the bottom of the ice, where the largest biomass concentrations are observed. Sea ice in McMurdo Sound is indeed considered as very productive, with an extremely high build-up of chl-*a* (Arrigo et al., 1995). Basal concentrations of chl-*a* reached up to 2,443 and 2,342 μg L^{-1} (stations YRS9 and YRS10, Figure 6a) and particulate organic carbon up to 2,600 μmol L^{-1}. This massive build-up of biomass associated with O_2 accumulation indicates autotrophy. According to the O_2/Ar ratio, autotrophy indeed dominated the bottom sea ice, but a transient heterotrophic period was observed between stations YRS8 and YRS11 (Figures 7c and 7d). Heterotrophy associated with biomass build-up has been reported earlier in the Arctic (Campbell et al., 2017; Rysgaard et al., 2008; Rysgaard & Glud, 2004). To the best of our knowledge, this is the first report of a large biomass build-up associated with a transient heterotrophic period in Antarctic sea ice. The best explanation for such a striking feature at the bottom of the ice is the rapid remineralization of the organic matter (Fripiat et al., 2014, 2017) entrapped within the biofilm (Roukaerts, 2018).

4.2. The Interior of the Sea Ice Cover

4.2.1. NCP

A significant imprint of biological processes on the oxygen pool can also be observed in the ice interior (Figure 8c). $NCP_{O2:Ar}$ in the ice interior exhibited the same temporal trend as in the bottom ice with dominant autotrophy (Figures 7c and 7d). NCP values in the interior ice were lower than in the bottom ice, in

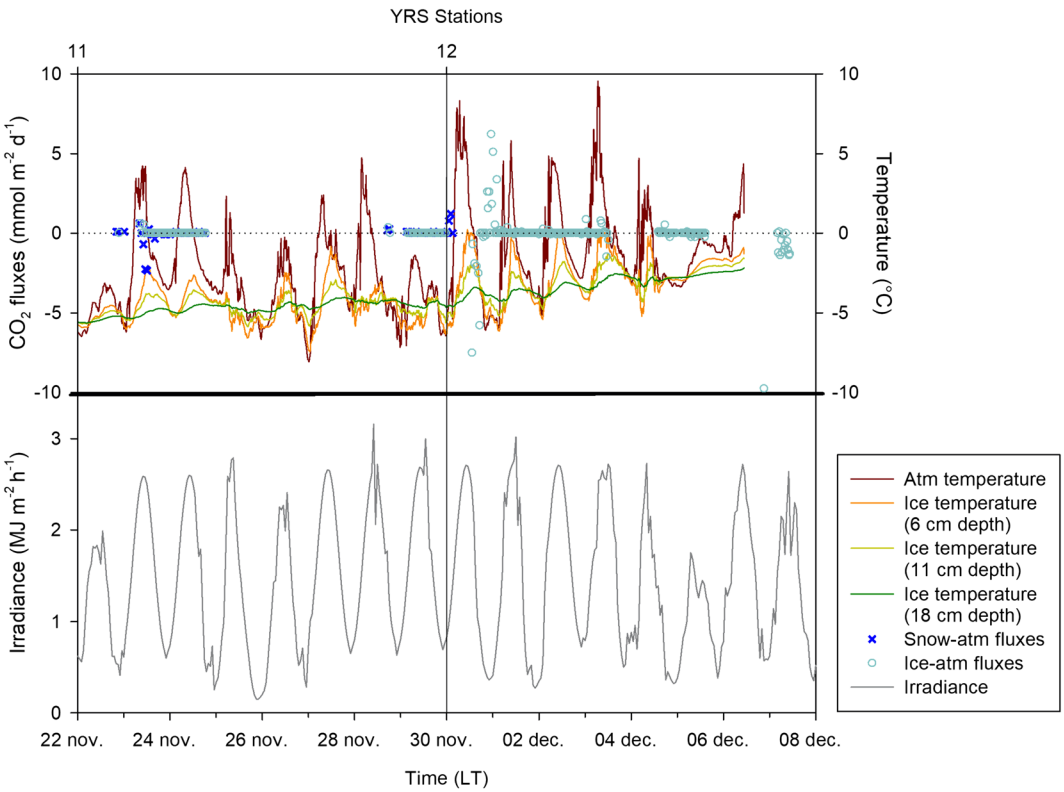

Figure 11. CO_2 fluxes in late spring (crosses for snow-atm fluxes and open circles for ice-atm fluxes), air temperature (brown line, recorded at 6 cm above the ice surface with ice-T buoy), ice temperatures (orange, yellow, and green lines, recorded at 6, 11, and 18 cm below the ice surface with ice-T buoy), and irradiance recorded at Arrival Heights (gray line).

agreement with biomass concentrations, except for stations YRS11 to YRS12. This higher NCP in the interior at stations YRS11 to YRS12 could be due to upward diffusion of biogenic oxygen enabled with the opening of the brine network (Zhou et al., 2013).

NCP_{DIC} in interior ice showed the same trophic dynamics (autotrophy vs. heterotrophy) as $NCP_{O2:Ar}$ except for stations YRS4–YRS6 and YRS10–YRS11. From stations YRS11 to YRS12, values agree within 3.4 mg C m^{-2} day^{-1}. The largest difference from stations YRS6 to YRS8 is 32 mg C m^{-2} day^{-1}. Overall, with the exception of stations YRS6 to YRS8, this suggests that biological activity was the main driver of DIC_6 temporal changes in the ice interior.

4.2.2. pCO_2 Gradient

Three temporal stages in pCO_2 dynamics have been identified based on physical parameters: (a) Supersaturation in the upper half of sea ice (stations YRS5 and YRS6) was observed during the winter-spring transition when brine contraction occurred due to cooling, leading to the concentration of salts, CO_2, and other gases associated with brine rejection and upward transport. (b) Surface undersaturation developed when the top layers become permeable, that is, when the BrV exceeded 5%, the theoretical permeability threshold for fluid transport through sea ice, according to Golden et al. (1998). pCO_2 at the ice surface decreases below saturation as a first consequence (YRS9 and YRS10). (c) Complete undersaturation of the ice column (stations YRS11, YRS12, and YRS3 even if preceded by 1 year) was observed by mid-November, with low sea ice pCO_2 as a consequence of ice melting and subsequent brine dilution, brine volume expansion, and increase in sea ice permeability.

4.3. The Surface of the Sea Ice Cover

4.3.1. Carbon Content

The dissolved inorganic carbon content of sea ice is affected by CO_2 exchanges. DIC_6 concentrations remained low (<351 μmol kg^{-1}) at the top of the ice (first 5 cm), compared to the ice interior. Such a

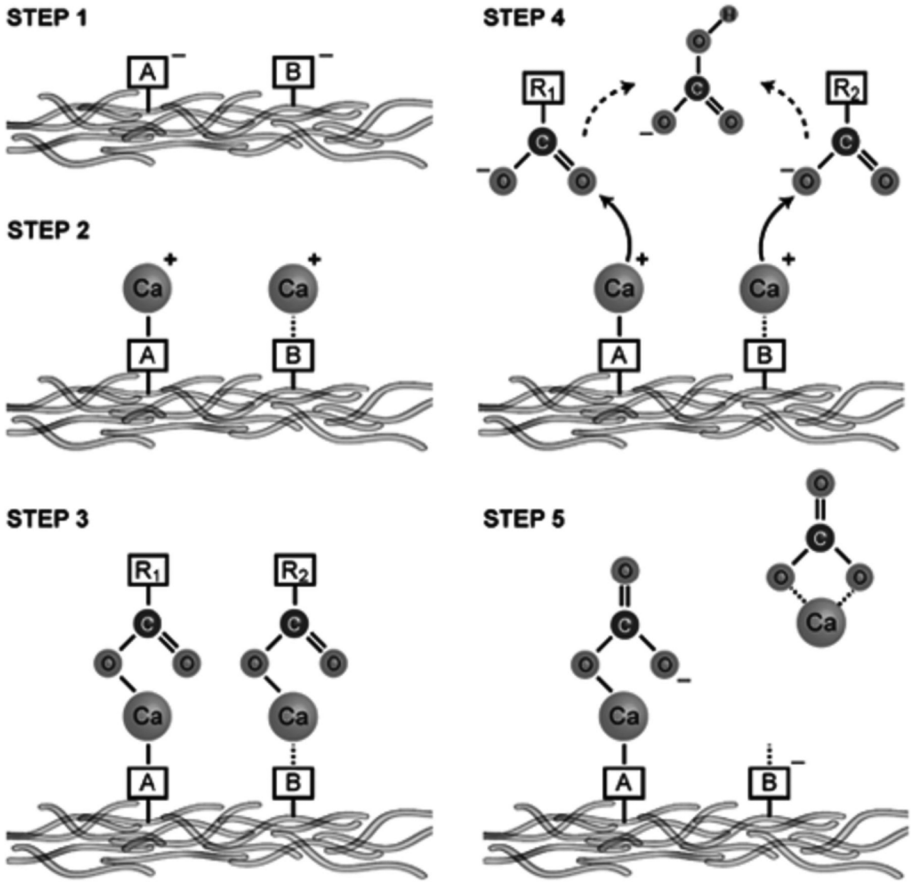

Figure 12. Conceptual model of calcium carbonate precipitation in the biofilm from Braissant et al. (2009). Step 1: EPS functional groups (A and B); step 2: calcium binding more or less tightly to functional groups A and B; step 3: complex formation between LMW organic carbon compound and calcium; step 4: release of LMW organic carbon by microbial activity and oxidation to HCO_3^- which in turn increases TA within the biofilm; step 5: $CaCO_3$ formation either on EPS or in pockets within the biofilm. Permission of Federation of European Microbiological Societies.

depletion at the top of the ice has been repeatedly observed (Geilfus et al., 2013; Kotovitch et al., 2016; Moreau et al., 2015). This depletion can be ascribed to the CO_2 release to the atmosphere since most primary production was concentrated at the bottom of the ice, and no significant calcium carbonate precipitation occurred at the sea ice surface except potentially at stations YRS11 and YRS12 (Figures 5c and 5d). CO_2 releases from the ice to the atmosphere occurred throughout all seasons, as explained in the next section.

Precipitation of calcium carbonate at the surface has been reported (Geilfus et al., 2013; Nomura et al., 2013; Rysgaard et al., 2013). The slight increase of $CaCO_3$ content at stations YRS11 and YRS12 (Figures 5c and 5d) indicates that precipitation develops at the ice surface consistently with omega ikaite above 1. During the rest of the survey, no precipitation was detected at the surface, while omega ikaite was lower and below 1 in cold surface ice (YRS5-YRS10).

4.3.2. pCO_2 and Air-Snow-Ice CO_2 Fluxes

CO_2 fluxes exhibited seasonal and diel variations and were likely affected by the thin wet and salty surface snow cover.

4.3.2.1. Seasonal Variations

The seasonal pattern of air-ice CO_2 fluxes direction was consistent with the pCO_2 evolution at the sea ice surface. CO_2 release generally occurred during the sea ice growth when pCO_2 was supersaturated (Figure 10). CO_2 uptake occurred mainly later in the season, during ice decay, when the ice became permeable (BrV > 5%), and pCO_2 was undersaturated. This seasonal pattern has also been reported by others (Delille

et al., 2014; Miller et al., 2011; Nomura et al., 2010; Papakyriakou & Miller, 2011). In late spring, fluxes were alternating between release and uptake on a short-time scale.

When the ice was expected to be impermeable during winter, that is, with brine volume at the sea ice surface below the permeability threshold for fluid transport of 5% (Golden et al., 1998), air-ice fluxes were generally close to zero. However, some significant CO_2 releases over snow-covered ice were observed. These significant winter CO_2 releases have been reported by others using eddy covariance techniques (Miller et al., 2011; Sievers et al., 2015). This questions the permeability threshold for gas transport in sea ice, permeability being a major control of CO_2 fluxes (Buckley & Trodahl, 1987; Delille et al., 2014). The gas permeability threshold is still debated and has been assessed for brine volumes ranging between 7.5% and 10% according to field observations (Zhou et al., 2013), while models suggest a threshold around 10% of brine volume (Moreau et al., 2014). However, at a smaller scale, the absence of discontinuity in the pCO_2 profiles (Figure S3) can argue for a permeability threshold below 5%.

Indeed, the principle of the pCO_2 measurement method is based on the equilibrium between the ice sample and the gas phase. Hence, the equilibrium depends on the ice permeability for gases. A first-order estimate of this permeability range is the same as the one for liquids (i.e., BrV > 5%). The method should not work below this threshold as reported by Geilfus, Carnat, et al. (2012) in sea ice from Barrow (AK) where pCO_2 in impermeable layers were constant around the concentration of the standard gas. Still, in this study, we carried out pCO_2 measurements for BrV < 5%. The trend was consistent below and within the range of liquid permeability, and the pCO_2 exceeded the standard gas concentration in impermeable layers, especially above 130 cm at stations YRS5 and YRS6 (Figure S3). As we did not observe the obvious bias reported by Geilfus, Carnat, et al. (2012) or any significant discontinuity in our pCO_2 profiles, our measurements seem to be valid below the 5% permeability threshold. This would suggest the BrV threshold for gas permeability to be lower than 5% in sea ice of McMurdo Sound. This calls for a better constraint of the permeability threshold for gases.

An alternative explanation for winter CO_2 efflux is the formation of microcracks in the landfast sea ice cover. Microcracking has been observed through acoustic studies in the Arctic (Dempsey et al., 2018; Milne, 1972) and Antarctica, especially in McMurdo Sound (Cole & Dempsey, 2004; Dempsey et al., 2018; Langhorne & Haskell, 1996). Ice cracking in the Arctic has been ascribed by Milne (1972) to thermal stress—temperature drop—in winter or spring. Temperature drops induce heat loss at the sea ice surface and subsequent tensile stresses (Ganton & Milne, 1965; Milne, 1972). Cracks, which relieve some of the stresses, are in turn produced along vertical planes and over tens of centimeters (Milne, 1972). Accordingly, visual observations carried out by Light et al. (2003) suggested large changes in microstructure as samples were cooled to −30°C and the presence of microcracks around inclusions while the ice cools and brines are expelled upward. This is consistent with the increase of pressure in sea ice related to ice cooling (Crabeck et al., 2016).

In this study, in early spring (27 September 2012), a sharp air temperature decrease (from −17°C to −25°C) was observed during the night (Figure 13). Ice temperatures followed the same trend and dropped from −17°C to −21°C. Simultaneously, CO_2 efflux up to 6 mmol m^{-2} day^{-1} occurred over the snow and the ice. This event is potentially linked to ice cracking. This calls for further investigation of the effect of microcracking on CO_2 release too.

4.3.2.2. Diel Variations in CO_2 Fluxes

In late spring, both release and uptake of CO_2 occurred over a 24 hr period. Uptake occurred when air and ice temperatures were above 0°C and −5°C, respectively, while release took place when temperatures dropped again below these levels at nighttime (Figure 11).

This diurnal pattern of CO_2 fluxes may be related to an increase of NCP during daylight and a decrease of NCP during nighttime. However, nighttime heterotrophy is questionable since solar irradiance was above 0.4 MJ m^{-2} hr^{-1} (Figure 11). Then CO_2 release at nighttime should also be ascribed to physical processes. The CO_2 release and uptake sequences could be related to diel temperature variations and the surface freeze-thaw cycles.

Atmospheric temperature variations were mainly affecting the top 6 cm of the ice (Figure 11). We assumed that the surface melt of sea ice was most likely occurring during day time. The subsequent brine dilution can lead to a large decrease of surface pCO_2 as observed at station YRS11 (sampled around midday) and allowed uptake of atmospheric CO_2. The nocturnal refreezing of the ice skin potentially induced CO_2 release to the

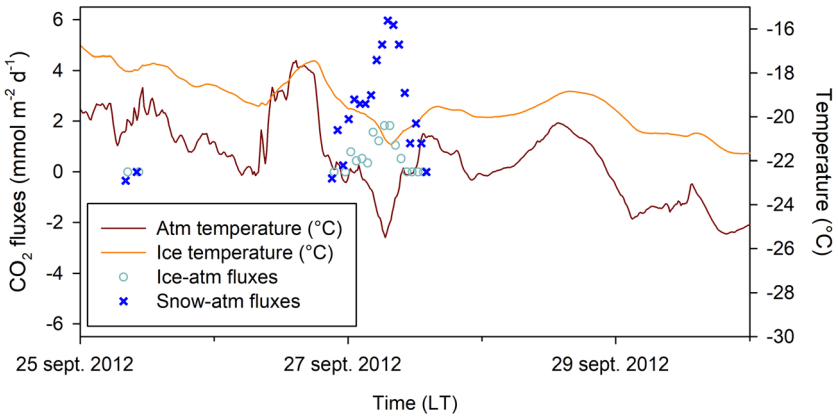

Figure 13. CO_2 fluxes in early spring, air temperature (brown line, recorded at 6 cm above the ice surface with ice-T buoy), and ice temperature (orange line, recorded at 6 cm below the ice surface with ice-T buoy).

atmosphere. Similarly, Papakyriakou and Miller (2011) observed prominent diurnal shifts from CO_2 release to CO_2 uptake over landfast sea ice using the eddy covariance technique. The uptake corresponded to local peaks in surface net radiation and air temperature while the release was associated with nighttime minima in net radiation and temperature. These authors ascribed the diel variations to cooling and freezing of the brines during the night.

Our results suggest that fluxes are highly variable on a diel cycle and that changes from release to uptake within 24 hr are likely linked to diel changes in NCP or freeze-thaw cycles during spring.

4.3.2.3. Effect of Thin Brine-Wetted Snow on CO_2 Fluxes

To date, only a few studies distinguished the snow-air interface and the ice-air interface. We observed larger CO_2 release over snow than over bare sea ice. Some studies have reported larger fluxes at the snow-air interface (Fischer, 2013; Geilfus, Delille, et al., 2012; Nomura et al., 2013), but in opposite others pointed out impeded CO_2 diffusion over snow-covered sea ice (Geilfus, Delille, et al., 2012; Meiners et al., 2018; Nomura, Yoshikawa-Inoue, et al., 2010). Indeed, deep snow cover may decrease the magnitude of the fluxes compared to bare ice, especially if superimposed ice—a fresh ice layer formed from snow meltwater—is forming (Delille et al., 2014; Geilfus, Delille, et al., 2012; Nomura, Yoshikawa-Inoue, et al., 2010; Zemmelink et al., 2006).

Early studies about fresh snow (i.e., snow without salt) over inland terrestrial ecosystems considered snow as an inert layer storing CO_2 and paid little attention to processes within the snow (Brooks et al., 2005; Takagi et al., 2005). Only the impact of biological processes (i.e., microbial respiration) has been studied and was reported not to be significant (Pirk et al., 2016). However, in terrestrial ecosystems close to the sea and even for sea ice, several studies reported chemical and photochemical reactions (see Bartels-Rausch et al., 2014, for a review). Sea salts in snow promote the formation of a surface liquid layer with a high ionic concentration that hosts chemical reactions (Domine & Shespon, 2002).

During this survey, neither snow ice nor superimposed ice formation that could act as a physical barrier to gas exchange were observed. The snow cover was characterized by high salinity (7.4–24.5), low thickness (below 4 cm), and high wetness due to brine wicking, that is, the upward migration of sea salt enriched brines from the sea ice to the snowpack (Domine et al., 2004). Compared to previous studies (Delille et al., 2014; Geilfus, Delille, et al., 2012; Nomura, Yoshikawa-Inoue, et al., 2010; Papakyriakou & Miller, 2011; Zemmelink et al., 2006), the snow cover was saltier and thinner during our survey. Wet and salty base snow can be viewed as solid snow crystals partially surrounded by liquid (i.e., brine) or disordered air-ice interface (Bartels-Rausch et al., 2014). Such a multiphase medium potentially modifies ice-gas interactions. First, gas adsorption or desorption on snow crystals is proportional to the specific surface area (SSA)—the surface area of snow accessible to gases per mass unit (Legagneux et al., 2002). SSA is changing with snow properties and types (e.g., temperature, density, morphology, and crystal structure). Gas interactions within wet snow cover are thus expected to be different from those within dry snow. In addition, CO_2 can

dissolve within this multiphase medium. Higher salinity increases the CO_2 buffer capacity of liquids or disordered layers, so that salty snow is likely to have a larger CO_2 storage capacity compared to fresh snow. The CO_2 storage capacity of salty base snow would add up to the total sea ice CO_2 storage capacity so that sea ice with a salty snow cover should have a larger CO_2 storage capacity compared to bare ice. We therefore suggest that the thin salty snow layer observed during the survey allowed CO_2 transport due to its shallowness and provided an enhanced CO_2 storage capacity compared to bare ice and related enhanced CO_2 fluxes.

5. Conclusions

We investigated the inorganic carbon dynamics in Antarctic landfast sea ice. Besides the first long-term monitoring of both pCO_2 and CO_2 fluxes at sea ice interfaces from winter to summer, this study also investigated the trophic status of sea ice and proposed a mechanism for calcium carbonate precipitation within the biofilm formed at the bottom of the ice.

Results revealed a succession of heterotrophic and autotrophic phases in the sea ice interior during spring. However, the seasonal pattern of CO_2 fluxes at the air-snow-ice interface was decoupled from the trophic status observed in the ice interior. This seasonal pattern of CO_2 fluxes was mainly driven by changes in pCO_2 at the surface that were related to physical processes. In late spring, diel variations of CO_2 fluxes were superimposed on seasonal variations. It appeared that both biotic and abiotic processes dominated the inorganic carbon dynamics at the sea ice surface in late spring. Diel variations potentially correspond to diel changes in NCP or to freeze-thaw cycles affecting basal snow and ice skin temperatures. As a result, a robust budget of air-snow-ice CO_2 fluxes would require both long-term and high-frequency measurements to capture both seasonal and diel patterns.

McMurdo landfast ice is known to accumulate a substantial amount of biomass and is recognized as one of the most productive biotopes of the global ocean. Accordingly, we observed a large biomass build-up at the bottom of the ice but, strikingly associated with transient heterotrophic activity and nitrate plus nitrite accumulation. This counterintuitive observation is likely due to the presence of a biofilm (microbial assemblages embedded in extracellular polymeric substances) where remineralization and accumulation of nutrients are taking place. Our results further suggest that such biofilm also promotes calcium carbonate precipitation, which develops in parallel with an increase of salinity-normalized TA, another counterintuitive observation. EPS functional groups within a biofilm can bind substantial amounts of free calcium. Sequential EPS degradation due to microbial activity create nucleation sites for calcium carbonate precipitation and provide bicarbonate ions within the biofilm that increase alkalinity. These observations call for further studies on the implication of biofilm formation at the bottom of sea ice.

Data Availability Statement

The data used within this work are available at the address: http://hdl.handle.net/2268/247284.

Acknowledgments

The authors would like to thank Brian Staite, Bernard Heinesch, Jiayun Zhou, Véronique Schoemann, Thomas Goossens, and the Scott Base crew for their assistance during fieldwork. We are indebted to Antarctica New Zealand for their logistical support. The authors are indebted to Nicolas-Xavier Geilfus and Elizabeth Jones for their detailed and constructive comments that greatly improved the overall quality of the manuscript. This research was supported by the FRS-FNRS (project YROSIAE, contract 2.4517.11), the Belgian Science Policy (project BIGSOUTH, contract SD/CA/05) and Antarctica New Zealand (project K131). Fanny Van der Linden, Marie Kotovitch, Sarah Wauthy, and Bruno Delille are PhD students and research associate, respectively, of the F.R.S.-FNRS.

References

Anderson, L. A. (1995). On the hydrogen and oxygen content of marine phytoplankton. *Deep-Sea Research Part I*, *42*(9), 1675–1680. https://doi.org/10.1016/0967-0637(95)00072-e

Arrigo, K., Dieckmann, G., Gosselin, M., Robinson, D., Fritsen, C., & Sullivan, C. (1995). High resolution study of the platelet ice ecosystem in McMurdo Sound, Antarctica: Biomass, nutrient, and production profiles within a dense microalgal bloom. *Marine Ecology Progress Series*, *127*, 255–268. https://doi.org/10.3354/meps127255

Assur, A. (1958). Composition of sea ice and its tensile strength. In *Arctic sea ice*, (pp. 106–138). Washington, DC: US National Academy of Sciences (National Research Council Publication 598).

Bartels-Rausch, T., Jacobi, H.-W., Kahan, T. F., Thomas, J. L., Thomson, E. S., Abbatt, J. P. D., et al. (2014). A review of air–ice chemical and physical interactions (AICI): Liquids, quasi-liquids, and solids in snow. *Atmospheric Chemistry and Physics*, *14*(3), 1587–1633. https://doi.org/10.5194/acp-14-1587-2014

Boetius, A., Anesio, A. M., Deming, J. W., Mikucki, J. A., & Rapp, J. Z. (2015). Microbial ecology of the cryosphere: Sea ice and glacial habitats. *Nature Reviews Microbiology*, *13*(11), 677–690. https://doi.org/10.1038/nrmicro3522

Braissant, O., Decho, A. W., Dupraz, C., Glunk, C., Przekop, K. M., & Visscher, P. T. (2007). Exopolymeric substances of sulfate-reducing bacteria: Interactions with calcium at alkaline pH and implication for formation of carbonate minerals. *Geobiology*, *5*(4), 401–411. https://doi.org/10.1111/j.1472-4669.2007.00117.x

Braissant, O., Decho, A. W., Przekop, K. M., Gallagher, K. L., Glunk, C., Dupraz, C., & Visscher, P. T. (2009). Characteristics and turnover of exopolymeric substances in a hypersaline microbial mat. *FEMS Microbiology Ecology*, *67*(2), 293–307. https://doi.org/10.1111/j.1574-6941.2008.00614.x

Brooks, P. D., McKnight, D., & Elder, K. (2005). Carbon limitation of soil respiration under winter snowpacks: Potential feedbacks between growing season and winter carbon fluxes. *Global Change Biology*, *11*(2), 231–238. https://doi.org/10.1111/j.1365-2486.2004.00877.x

Brown, K. A., Miller, L. A., Davelaar, M., Francois, R., & Tortell, P. D. (2014). Over-determination of the carbonate system in natural sea-ice brine and assessment of carbonic acid dissociation constants under low temperature, high salinity conditions. *Marine Chemistry*, *165*, 36–45. https://doi.org/10.1016/j.marchem.2014.07.005

Brown, K. A., Miller, L. A., Mundy, C. J., Papakyriakou, T., Francois, R., Gosselin, M., et al. (2015). Inorganic carbon system dynamics in landfast Arctic sea ice during the early-melt period. *Journal of Geophysical Research: Oceans*, *120*, 3542–3566. https://doi.org/10.1002/2014JC010620

Buckley, R. G., & Trodahl, H. J. (1987). Thermally driven changes in the optical properties of sea ice. *Cold Regions Science and Technology*, *14*(2), 201–204. https://doi.org/10.1016/0165-232x(87)90036-x

Campbell, K., Mundy, C. J., Gosselin, M., Landy, J. C., Delaforge, A., & Rysgaard, S. (2017). Net community production in the bottom of first-year sea ice over the Arctic spring bloom. *Geophysical Research Letters*, *44*, 8971–8978. https://doi.org/10.1002/2017GL074602

Carnat, G., Papakyriakou, T., Geilfus, N. X., Brabant, F., Delille, B., Vancoppenolle, M., et al. (2013). Investigations on physical and textural properties of arctic first-year sea ice in the Amundsen gulf, Canada, November 2007-June 2008 (IPY-CFL system study). *Journal of Glaciology*, *59*(217), 819–837. https://doi.org/10.3189/2013JoG12J148

Carnat, G., Said-Ahmad, W., Fripiat, F., Wittek, B., Tison, J.-L., Uhlig, C., & Amrani, A. (2018). Variability in sulfur isotope composition suggests unique dimethylsulfoniopropionate cycling and microalgae metabolism in Antarctic sea ice. *Communications Biology*, *1*(1), 212. https://doi.org/10.1038/s42003-018-0228-y

Carnat, G., Zhou, J., Papakyriakou, T., Delille, B., Goossens, T., Haskell, T., et al. (2014). Physical and biological controls on DMS,P dynamics in ice shelf-influenced fast ice during a winter-spring and a spring-summer transitions. *Geophysical Research Letters*, *119*, 2882–2905. https://doi.org/10.1002/2013JC009381

Cole, D. M., & Dempsey, J. P. (2004). In situ sea ice experiments in McMurdo Sound: Cyclic loading, fracture, and acoustic emissions. *Journal of Cold Regions Engineering*, *18*(4), 155–174. https://doi.org/10.1061/(ASCE)0887-381X(2004)18:4(155)

Cox, G. F. N., & Weeks, W. F. (1983). Equations for determining the gas and brine volumes in sea-ice samples. *Journal of Glaciology*, *29*(102), 306–316. https://doi.org/10.3189/S0022143000008364

Cox, G. F. N., & Weeks, W. F. (1986). Changes in the salinity and porosity of sea-ice samples during shipping and storage. *Journal of Glaciology*, *32*(112), 371–375. https://doi.org/10.3189/S0022143000012065

Crabeck, O., Delille, B., Thomas, D. N., Geilfus, N.-X. N.-X., Rysgaard, S., & Tison, J.-L. J.-L. (2014). CO_2 and CH_4 in sea ice from a subarctic fjord under influence of riverine input. *Biogeosciences*, *11*(23), 6525–6538. https://doi.org/10.5194/bg-11-6525-2014

Crabeck, O., Galley, R., Delille, B., Else, B., Geilfus, N.-X., Lemes, M., et al. (2016). Imaging air volume fraction in sea ice using non-destructive X-ray tomography. *The Cryosphere*, *10*(3), 1125–1145. https://doi.org/10.5194/tc-10-1125-2016

Decho, A. W. (2000). Microbial biofilms in intertidal systems: An overview. *Continental Shelf Research*, *20*(10–11), 1257–1273. https://doi.org/10.1016/s0278-4343(00)00022-4

Decho, A. W., & Gutierrez, T. (2017). Microbial extracellular polymeric substances (EPSs) in ocean systems. *Frontiers in Microbiology*, *8*, 922. https://doi.org/10.3389/fmicb.2017.00922

Delille, B., Harlay, J., Zondervan, I., Jacquet, S., Chou, L., Wollast, R., et al. (2005). Response of primary production and calcification to changes of pCO_2 during experimental blooms of the coccolithophorid *Emiliania huxleyi*. *Global Biogeochemical Cycles*, *19*(2), 1–14. https://doi.org/10.1029/2004GB002318

Delille, B., Jourdain, B., Borges, A. V., Tison, J.-L., & Delille, D. (2007). Biogas (CO_2, O_2, dimethylsulfide) dynamics in spring Antarctic fast ice. *Limnology and Oceanography*, *52*(4), 1367–1379. https://doi.org/10.4319/lo.2007.52.4.1367

Delille, B., Vancoppenolle, M., Geilfus, N.-X., Tilbrook, B., Lannuzel, D., Schoemann, V., et al. (2014). Southern Ocean CO_2 sink: The contribution of the sea ice. *Journal of Geophysical Research: Oceans*, *119*, 6340–6355. https://doi.org/10.1002/2014JC009941

Deming, J. W. (2007). Life in ice formations at very cold temperatures. In *Physiology and biochemistry of extremophiles* (pp. 133–144). Washington, DC: American Society of Microbiology.

Deming, J. W. (2010). Sea ice bacteria and viruses. In D. N. Thomas, & G. S. Dieckmann (Eds.), *Sea ice*, (pp. 247–282). Oxford, UK: Wiley-Blackwell.

Dempsey, J. P., Cole, D. M., & Wang, S. (2018). Tensile fracture of a single crack in first-year sea ice. *Philosophical Transactions of the Royal Society A: Mathematical, Physical and Engineering Sciences*, *376*(2129), 20170346. https://doi.org/10.1098/rsta.2017.0346

DOE (1994). In A. G. Dickson & C. Goyet (Eds.), *Handbook of methods for the analysis of the various parameters of the carbon dioxide system in sea water. Version 2*. Oak Ridge, TN: ORNL/CDIAC-74. https://doi.org/10.2172/10107773

Dieckmann, G. S., Nehrke, G., Papadimitriou, S., Göttlicher, J., Steininger, R., Kennedy, H., et al. (2008). Calcium carbonate as ikaite crystals in Antarctic sea ice. *Geophysical Research Letters*, *35*, L08501. https://doi.org/10.1029/2008GL033540

Domine, F., & Shespon, P. (2002). Air-snow interactions and atmospheric chemistry. *Science*, *297*(5586), 1506–1510. https://doi.org/10.1126/science.1074610

Domine, F., Sparapani, R., Ianniello, A., & Beine, H. J. (2004). The origin of sea salt in snow on Arctic sea ice and in coastal regions. *Atmospheric Chemistry and Physics*, *4*(9/10), 2259–2271. https://doi.org/10.5194/acp-4-2259-2004

Eicken, H., & Lange, M. (1991). Image analysis of sea-ice thin sections: A step towards automated texture classification. *Annals of Glaciology*, *15*, 204–209. https://doi.org/10.1017/S0260305500009745

Fischer, M. (2013). *Sea ice and the air-sea exchange of CO_2 (doctoral dissertation)*. Bremen: Bremen University. Retrieved from https://elib.suub.uni-bremen.de/edocs/00103066-1.pdf

Fripiat, F., Meiners, K. M., Vancoppenolle, M., Papadimitriou, S., Thomas, D. N., Ackley, S. F., et al. (2017). Macro-nutrient concentrations in Antarctic pack ice: Overall patterns and overlooked processes. *Elementa: Science of the Anthropocene*, *5*(0), 13. https://doi.org/10.1525/elementa.217

Fripiat, F., Sigman, D. M., Fawcett, S. E., Rafter, P. A., Weigand, M. A., & Tison, J.-L. (2014). New insights into sea ice nitrogen biogeochemical dynamics from the nitrogen isotopes. *Global Biogeochemical Cycles*, *28*(2), 115–130. https://doi.org/10.1002/2013GB004729

Ganton, J. H., & Milne, A. R. (1965). Temperature- and wind-dependent ambient noise under midwinter pack ice. *The Journal of the Acoustical Society of America*, *38*(3), 406–411. https://doi.org/10.1121/1.1909697

Garcia, H. E., & Gordon, L. I. (1992). Oxygen solubility in seawater: Better fitting equations. *Limnology and Oceanography*, *37*(6), 1307–1312. https://doi.org/10.4319/lo.1992.37.6.1307

Geilfus, N.-X., Carnat, G., Dieckmann, G. S., Halden, N., Nehrke, G., Papakyriakou, T., et al. (2013). First estimates of the contribution of $CaCO_3$ precipitation to the release of CO_2 to the atmosphere during young sea ice growth. *Journal of Geophysical Research: Oceans*, *118*(1), 244–255. https://doi.org/10.1029/2012JC007980

Geilfus, N.-X., Carnat, G., Papakyriakou, T., Tison, J. L., Else, B., Thomas, H., et al. (2012). Dynamics of pCO_2 and related air-ice CO_2 fluxes in the Arctic coastal zone (Amundsen gulf, Beaufort Sea). *Journal of Geophysical Research*, *117*. https://doi.org/10.1029/2011JC007118

Geilfus, N.-X., Delille, B., Verbeke, V., & Tison, J. (2012). Towards a method for high vertical resolution measurements of the partial pressure of CO_2 within bulk sea ice. *Journal of Glaciology*, *58*(208), 287–300. https://doi.org/10.3189/2012JoG11J071

Geilfus, N.-X., Galley, R. J., Crabeck, O., Papakyriakou, T., Landy, J., Tison, J.-L., & Rysgaard, S. (2015). Inorganic carbon dynamics of melt-pond-covered first-year sea ice in the Canadian Arctic. *Biogeosciences*, *12*(6), 2047–2061. https://doi.org/10.5194/bg-12-2047-2015

Geilfus, N.-X., Tison, J.-L., Ackley, S. F., Galley, R. J., Rysgaard, S., Miller, L. A., & Delille, B. (2014). Sea ice pCO_2 dynamics and air—Ice CO_2 fluxes during the sea ice mass balance in the Antarctic (SIMBA) experiment—Bellingshausen Sea, Antarctica. *The Cryosphere*, *8*(6), 2395–2407. https://doi.org/10.5194/tc-8-2395-2014

Glud, R., Rysgaard, S., & Kühl, M. (2002). A laboratory study on O_2 dynamics and photosynthesis in ice algal communities: Quantification by microsensors, O_2 exchange rates, ^{14}C incubations and a PAM fluorometer. *Aquatic Microbial Ecology*, *27*, 301–311. https://doi.org/10.3354/ame027301

Golden, K. M., Ackley, S. F., & Lytle, V. I. (1998). The percolation phase transition in sea ice. *Science*, *282*(5397), 2238–2241. https://doi.org/10.1126/science.282.5397.2238

Goyet, C., & Poisson, A. (1989). New determination of carbonic acid dissociation constants in seawater as a function of temperature and salinity. *Deep Sea Research Part A. Oceanographic Research Papers*, *36*(11), 1635–1654. https://doi.org/10.1016/0198-0149(89)90064-2

Gran, G. (1952). Determination of the equivalence point in potentiometric titrations part II. *Analyst*, *77*(920), 661–671. https://doi.org/10.1039/AN9527700661

Gruber, N., Landschützer, P., & Lovenduski, N. S. (2019). The variable Southern Ocean carbon sink. *Annual Review of Marine Science*, *11*(1), 159–186. https://doi.org/10.1146/annurev-marine-121916-063407

Hamme, R., & Emerson, S. (2004). The solubility of neon, nitrogen and argon in distilled water and seawater. *Deep Sea Research Part I Oceanographic Research Papers*, *51*(11), 1517–1528. https://doi.org/10.1016/j.dsr.2004.06.009

Helmke, E., & Weyland, H. (1995). Bacteria in sea ice and underlying water of the eastern Weddell Sea in midwinter. *Marine Ecology Progress Series*, *117*(1–3), 269–287. https://doi.org/10.3354/meps117269

Horner, R., Ackley, S., Dieckmann, G., Gulliksen, B., Hoshiai, T., Legendre, L., et al. (1992). Ecology of sea ice biota. *Polar Biology*, *12*(3–4), 417–427. https://doi.org/10.1007/BF00243113

Huston, A. L., Krieger-Brockett, B. B., & Deming, J. W. (2000). Remarkably low temperature optima for extracellular enzyme activity from Arctic bacteria and sea ice. *Environmental Microbiology*, *2*(4), 383–388. https://doi.org/10.1046/j.1462-2920.2000.00118.x

Jeffries, M. O., Weeks, W. F., Shaw, R., & Morris, K. (1993). Structural characteristics of congelation and platelet ice and their role in the development of antarctic land-fast sea ice. *Journal of Glaciology*, *39*(132), 223–238. https://doi.org/10.3189/S0022143000015884

Kotovitch, M., Moreau, S., Zhou, J., Vancoppenolle, M., Dieckmann, G. S., Evers, K.-U., et al. (2016). Air-ice carbon pathways inferred from a sea ice tank experiment. *Elementa: Science of the Anthropocene*, *4*, 000112. https://doi.org/10.12952/journal.elementa.000112

Krembs, C., & Engel, A. (2001). Abundance and variability of microorganisms and transparent exopolymer particles across the ice-water interface of melting first-year sea ice in the Laptev Sea (Arctic). *Marine Biology*, *138*(1), 173–185. https://doi.org/10.1007/s002270000396

Langhorne, P. J., & Haskell, T. G. (1996). Acoustic emission during fatigue experiments on first year sea ice. *Cold Regions Science and Technology*, *24*(3), 237–250. https://doi.org/10.1016/0165-232X(95)00021-3

Langway, C. C. (1958). *Ice fabrics and the universal stage* (pp. 1–17). United States: Army Snow Ice and Permafrost Research Establishment, (snow ice and permafrost research establishment).

Legagneux, L., Cabanes, A., & Dominé, F. (2002). Measurement of the specific surface area of 176 snow samples using methane adsorption at 77 K. *Journal of Geophysical Research*, *107*(D17), ACH 5-1–ACH 5-15. https://doi.org/10.1029/2001JD001016

Leonard, G. H., Purdie, C. R., Langhorne, P. J., Haskell, T. G., Williams, M. J. M., & Frew, R. D. (2006). Observations of platelet ice growth and oceanographic conditions during the winter of 2003 in McMurdo Sound, Antarctica. *Journal of Geophysical Research*, *111*. https://doi.org/10.1029/2005JC002952

Leppäranta, M., & Manninen, T. (1988). *The brine and gas content of sea ice with attention to low salinities and high temperatures*. Helsinki, Finland. Retrieved from http://aquaticcommons.org/id/eprint/6760

Lewis, E., & Wallace, D. (1998). *Program developed for CO_2 system calculations*. Oak Ridge, TN: ORNL/CDIAC-105.

Light, B., Maykut, G. A., & Grenfell, T. C. (2003). Effects of temperature on the microstructure of first-year Arctic sea ice. *Journal of Geophysical Research*, *108*(C2). https://doi.org/10.1029/2001JC000887

Luhtanen, A., Eronen-rasimus, E., Oksanen, H. M., Tison, J., Delille, B., Dieckmann, G. S., et al. (2018). The first known virus isolates from Antarctic sea ice have complex infection patterns. *FEMS Microbiology Ecology*, *94*(4), 1–15. https://doi.org/10.1093/femsec/fiy028

Massom, R. A., Eicken, H., Hass, C., Jeffries, M. O., Drinkwater, M. R., & Sturm, M. (2001). Snow on Antarctic sea ice. *Reviews of Geophysics*, *39*(3), 413–445. https://doi.org/10.1029/2000RG000085

McMinn, A., Ashworth, C., Bhagooli, R., Martin, A., Salleh, S., Ralph, P., & Ryan, K. (2012). Antarctic coastal microalgal primary production and photosynthesis. *Marine Biology*, *159*(12), 2827–2837. https://doi.org/10.1007/s00227-012-2044-0

Meiners, K., Gradinger, R., Fehling, J., Civitarese, G., & Spindler, M. (2003). Vertical distribution of exopolymer particles in sea ice of the Fram Strait (Arctic) during autumn. *Marine Ecology Progress Series*, *248*, 1–13. https://doi.org/10.3354/meps248001

Meiners, K. M., Krembs, C., & Gradinger, R. (2008). Exopolymer particles: Microbial hotspots of enhanced bacterial activity in Arctic fast ice (Chukchi Sea). *Aquatic Microbial Ecology*, *52*, 195–207. https://doi.org/10.3354/ame01214

Meiners, K. M., Vancoppenolle, M., Carnat, G., Castellani, G., Delille, B., Delille, D., et al. (2018). Chlorophyll-a in Antarctic landfast sea ice: A first synthesis of historical ice core data. *Journal of Geophysical Research: Oceans*, *123*, 8444–8459. https://doi.org/10.1029/2018JC014245

Miller, L. A., Papakyriakou, T. N., Collins, R. E., Deming, J. W., Ehn, J. K., Macdonald, R. W., et al. (2011). Carbon dynamics in sea ice: A winter flux time series. *Journal of Geophysical Research*, *116*, C02028. https://doi.org/10.1029/2009JC006058

Milne, A. R. (1972). Thermal tension cracking in sea ice: A source of underice noise. *Journal of Geophysical Research*, *77*(12), 2177–2192. https://doi.org/10.1029/JC077i012p02177

Moreau, S., Vancoppenolle, M., Delille, B., Tison, J.-L., Zhou, J., Kotovitch, M., et al. (2015). Drivers of inorganic carbon dynamics in first-year sea ice: A model study. *Journal of Geophysical Research: Oceans*, *120*, 471–495. https://doi.org/10.1002/2014JC010388

Moreau, S., Vancoppenolle, M., Zhou, J., Tison, J. L., Delille, B., & Goosse, H. (2014). Modelling argon dynamics in first-year sea ice. *Ocean Modelling*, *73*, 1–18. https://doi.org/10.1016/j.ocemod.2013.10.004

NOAA (1976). U.S. standard atmosphere, 1976. National Oceanic and Amospheric administration.

Nomura, D., Assmy, P., Nehrke, G., Granskog, M. A., Fischer, M., Dieckmann, G. S., et al. (2013). Characterization of ikaite ($CaCO_3 \cdot 6H_2O$) crystals in first-year Arctic sea ice north of Svalbard. *Annals of Glaciology*, *54*(62), 125–131. https://doi.org/10.3189/2013AoG62A034

Nomura, D., Eicken, H., Gradinger, R., & Shirasawa, K. (2010). Rapid physically driven inversion of the air–sea ice CO_2 flux in the seasonal landfast ice off Barrow, Alaska after onset of surface melt. *Continental Shelf Research*, *30*(19), 1998–2004. https://doi.org/10.1016/j.csr.2010.09.014

Nomura, D., Granskog, M. A., Fransson, A., Chierici, M., Silyakova, A., Ohshima, K. I., et al. (2018). CO_2 flux over young and snow-covered Arctic pack ice in winter and spring. *Biogeosciences*, *15*(11), 3331–3343. https://doi.org/10.5194/bg-15-3331-2018

Nomura, D., Yoshikawa-Inoue, H., Toyota, T., & Shirasawa, K. (2010). Effects of snow, snowmelting and refreezing processes on air–sea-ice CO_2 flux. *Journal of Glaciology*, *56*(196), 262–270. https://doi.org/10.3189/002214310791968548

Notz, D. (2005). *Thermodynamic and fluid-dynamical processes in sea ice (doctoral dissertation)*. Cambridge: University of Cambridge. Retrieved from http://mpimet.mpg.de/fileadmin/staff/notzdirk/Notz_PhD_abstract.pdf

Notz, D., & Worster, M. G. (2008). In situ measurements of the evolution of young sea ice. *Journal of Geophysical Research*, *113*, C03001. https://doi.org/10.1029/2007JC004333

Papadimitriou, S., Kennedy, H., Kennedy, P., & Thomas, D. N. (2013). Ikaite solubility in seawater-derived brines at 1atm and sub-zero temperatures to 265K. *Geochimica et Cosmochimica Acta*, *109*, 241–253. https://doi.org/10.1016/j.gca.2013.01.044

Papadimitriou, S., Kennedy, H., Norman, L., Kennedy, D. P., Dieckmann, G. S., & Thomas, D. N. (2012). The effect of biological activity, $CaCO_3$ mineral dynamics, and CO_2 degassing in the inorganic carbon cycle in sea ice in late winter-early spring in the Weddell Sea, Antarctica. *Journal of Geophysical Research*, *117*, C08011. https://doi.org/10.1029/2012JC008058

Papakyriakou, T., & Miller, L. (2011). Springtime CO_2 exchange over seasonal sea ice in the Canadian Arctic archipelago. *Annals of Glaciology*, *52*(57), 215–224. https://doi.org/10.3189/172756411795931534

Pirk, N., Tamstorf, M. P., Lund, M., Mastepanov, M., Pedersen, S. H., Mylius, M. R., et al. (2016). Snowpack fluxes of methane and carbon dioxide from high Arctic tundra. *Journal of Geophysical Research: Biogeosciences*, *121*, 2886–2900. https://doi.org/10.1002/2016JG003486

Poulin, M., Daugbjerg, N., Gradinger, R., Ilyash, L., Ratkova, T., & von Quillfeldt, C. (2011). The pan-Arctic biodiversity of marine pelagic and sea-ice unicellular eukaryotes: A first-attempt assessment. *Marine Biodiversity*, *41*(1), 13–28. https://doi.org/10.1007/s12526-010-0058-8

Raynaud, D., Delmas, R., Ascencio, J. M., & Legrand, M. (1982). Gas extraction from polar ice cores: A critical issue for studying the evolution of atmospheric CO_2 and ice-sheet surface elevation. *Annals of Glaciology*, *3*, 265–268. https://doi.org/10.3189/S0260305500002895

Reuer, M. K., Barnett, B. A., Bender, M. L., Falkowski, P. G., & Hendricks, M. B. (2007). New estimates of Southern Ocean biological production rates from O_2/Ar ratios and the triple isotope composition of O_2. *Deep Sea Research Part I: Oceanographic Research Papers*, *54*(6), 951–974. https://doi.org/10.1016/j.dsr.2007.02.007

Riedel, A., Michel, C., & Gosselin, M. (2006). Seasonal study of sea-ice exopolymeric substances on the Mackenzie shelf: Implications for transport of sea-ice bacteria and algae. *Aquatic Microbial Ecology*, *45*(2), 195–206. https://doi.org/10.3354/ame045195

Riedel, A., Michel, C., Gosselin, M., & LeBlanc, B. (2007). Enrichment of nutrients, exopolymeric substances and microorganisms in newly formed sea ice on the Mackenzie shelf. *Marine Ecology Progress Series*, *342*, 55–67. https://doi.org/10.3354/meps342055

Roukaerts, A. (2018). *Novel insights in nitrogen and carbon biogeochemistry of Antarctic sea ice: The potential role of a microbial biofilm (doctoral dissertation)*. Brussels: Vrije Universiteit Brussel.

Rysgaard, S., Bendtsen, J., Delille, B., Dieckmann, G. S., Glud, R. N., Kennedy, H., et al. (2011). Sea ice contribution to the air–sea CO_2 exchange in the Arctic and southern oceans. *Tellus B*, *63*(5), 823–830. https://doi.org/10.1111/j.1600-0889.2011.00571.x

Rysgaard, S., & Glud, R. N. (2004). Anaerobic N_2 production in Arctic sea ice. *Limnology and Oceanography*, *49*(1), 86–94. https://doi.org/10.4319/lo.2004.49.1.0086

Rysgaard, S., Glud, R. N., Sejr, M. K., Bendtsen, J., & Christensen, P. B. (2007). Inorganic carbon transport during sea ice growth and decay: A carbon pump in polar seas. *Journal of Geophysical Research*, *112*, C03016. https://doi.org/10.1029/2006JC003572

Rysgaard, S., Glud, R. N., Sejr, M. K., Blicher, M. E., & Stahl, H. J. (2008). Denitrification activity and oxygen dynamics in Arctic sea ice. *Polar Biology*, *31*(5), 527–537. https://doi.org/10.1007/s00300-007-0384-x

Rysgaard, S., Søgaard, D. H., Cooper, M., Pućko, M., Lennert, K., Papakyriakou, T. N., et al. (2013). Ikaite crystal distribution in winter sea ice and implications for CO_2 system dynamics. *The Cryosphere*, *7*(2), 707–718. https://doi.org/10.5194/tc-7-707-2013

Sievers, J., Sørensen, L. L., Papakyriakou, T., Else, B., Sejr, M. K., Haubjerg Søgaard, D., et al. (2015). Winter observations of CO_2 exchange between sea ice and the atmosphere in a coastal fjord environment. *The Cryosphere*, *9*(4), 1701–1713. https://doi.org/10.5194/tc-9-1701-2015

Søgaard, D., Kristensen, M., Rysgaard, S., Glud, R., Hansen, P., & Hilligsøe, K. (2010). Autotrophic and heterotrophic activity in Arctic first-year sea ice: Seasonal study from Malene bight, SW Greenland. *Marine Ecology Progress Series*, *419*, 31–45. https://doi.org/10.3354/meps08845

Stefels, J., Carnat, G., Dacey, J. W. H., Goossens, T., Elzenga, J. T. M., & Tison, J.-L. (2012). The analysis of dimethylsulfide and dimethylsulfoniopropionate in sea ice: Dry-crushing and melting using stable isotope additions. *Marine Chemistry*, *128-129*, 34–43. https://doi.org/10.1016/j.marchem.2011.09.007

Stewart, P. S. (2003). Diffusion in biofilms. *Journal of Bacteriology*, *185*(5), 1485 LP–1491. https://doi.org/10.1128/JB.185.5.1485-1491.2003

Stewart, P. S., & Franklin, M. J. (2008). Physiological heterogeneity in biofilms. *Nature Reviews Microbiology*, *6*(3), 199–210. https://doi.org/10.1038/nrmicro1838

Takagi, K., Nomura, M., Ashiya, D., Takahashi, H., Sasa, K., Fujinuma, Y., et al. (2005). Dynamic carbon dioxide exchange through snowpack by wind-driven mass transfer in a conifer-broadleaf mixed forest in northernmost Japan. *Global Biogeochemical Cycles*, *19*(2). https://doi.org/10.1029/2004GB002272

Takahashi, T., Sutherland, S. C., Sweeney, C., Poisson, A., Metzl, N., Tilbrook, B., et al. (2002). Global Sea–air CO_2 flux based on climatological surface ocean pCO_2, and seasonal biological and temperature effects. *Deep Sea Research Part II: Topical Studies in Oceanography*, *49*(9–10), 1601–1622. https://doi.org/10.1016/S0967-0645(02)00003-6

Thomas, D. N., & Dieckmann, G. S. (2010). *Sea ice*, (2nd ed.). Oxford, UK: Wiley-Blackwell.

Tison, J.-L., Lorrain, R. D., Bouzette, A., Dini, M., Bondesan, A., & StiéVenard, M. (2013). Linking landfast sea ice variability to marine ice accretion at hells gate ice shelf, Ross Sea. In *Antarctic sea ice: Physical processes, interactions and variability* (pp. 375–407). Washington, DC. https://doi.org/10.1029/AR074p0375

UNESCO (1966). *International oceanographic tables*. Paris: National Institute of Oceanography of Great Britain and UNESCO.

Vancoppenolle, M., Notz, D., Vivier, F., Tison, J., Delille, B., Carnat, G., et al. (2013). Technical note: On the use of the mushy-layer Rayleigh number for the interpretation of sea-ice-core data. *The Cryosphere Discuss*, *7*(4), 3209–3230. https://doi.org/10.5194/tcd-7-3209-2013

Verbeke, V. (2005). *Concentrations en gaz dans la glace de mer: développements techniques et implications environnementales (Doctoral dissertation)*. Brussels: Université Libre de Bruxelles. Retrieved from http://hdl.handle.net/2013/ULB-DIPOT:oai:dipot.ulb.ac.be:2013/210942

Zemmelink, H. J., Delille, B., Tison, J.-L., Hintsa, E. J., Houghton, L., & Dacey, J. W. H. (2006). CO_2 deposition over the multi-year ice of the western Weddell Sea. *Geophysical Research Letters*, *33*, L13606. https://doi.org/10.1029/2006gl026320

Zhou, J., Delille, B., Brabant, F., & Tison, J.-L. (2014). Insights into oxygen transport and net community production in sea ice from oxygen, nitrogen and argon concentrations. *Biogeosciences*, *11*(18), 5007–5020. https://doi.org/10.5194/bg-11-5007-2014

Zhou, J., Delille, B., Eicken, H., Vancoppenolle, M., Brabant, F., Carnat, G., et al. (2013). Physical and biogeochemical properties in landfast sea ice (Barrow, Alaska): Insights on brine and gas dynamics across seasons. *Journal of Geophysical Research, Oceans*, *118*(6), 3172–3189. https://doi.org/10.1002/jgrc.20232